

AD-A118 614

CALIFORNIA UNIV DAVIS DEPT OF MECHANICAL ENGINEERING F/G 11/6
FUNDAMENTAL INVESTIGATIONS OF SUPERPLASTIC FORMING PROCESSES.(U)
MAR 82 A K MUKHERJEE, A ARIELI AFOSR-79-0069

UNCLASSIFIED

AFOSR-TR-82-0677

NL

For /

of /

the /

END

DATE

9 82

DTIC

UNCLASSIFIED

SECURITY CLASSIFICATION OF THIS PAGE (When Data Entered)

AD A118614

DTIC FILE COPY

REPORT DOCUMENTATION PAGE		READ INSTRUCTIONS BEFORE COMPLETING FORM
1. REPORT NUMBER AFOSR-TR- 82 - 0677	2. GOVT ACCESSION NO. AD-A118614	3. RECIPIENT'S CATALOG NUMBER
4. TITLE (and Subtitle) Fundamental Investigations of Superplastic Forming Processes		5. TYPE OF REPORT & PERIOD COVERED Final Scientific Report 2/1/79 to 1/31/82
7. AUTHOR(s) A. K. Mukherjee & A. Arieli		6. PERFORMING ORG. REPORT NUMBER
9. PERFORMING ORGANIZATION NAME AND ADDRESS Div. of Materials Science & Engineering Department of Mechanical Engineering Univ. of California, Davis, CA 95616		8. CONTRACT OR GRANT NUMBER(s) AFOSR-79-0069
11. CONTROLLING OFFICE NAME AND ADDRESS AFOSR/NE, Building 410 Bolling Air Force Base, D.C. 20332		10. PROGRAM ELEMENT, PROJECT, TASK AREA & WORK UNIT NUMBERS 6-1102F 2306/A1
14. MONITORING AGENCY NAME & ADDRESS (if different from Controlling Office)		12. REPORT DATE March 1982
		13. NUMBER OF PAGES 73
		15. SECURITY CLASS. (of this report) Unclassified
		15a. DECLASSIFICATION/DOWNGRADING SCHEDULE
16. DISTRIBUTION STATEMENT (of this Report) Approved for public release; distribution unlimited.		
17. DISTRIBUTION STATEMENT (of the abstract entered in Block 20, if different from Report) DTIC ELECTE S AUG 26 1982 F		
18. SUPPLEMENTARY NOTES To be published in part in <i>Acta Metallurgica</i>		
19. KEY WORDS (Continue on reverse side if necessary and identify by block number) Superplasticity, mechanical behavior, deformation mechanisms, three-dimensional deformation mechanism map		
20. ABSTRACT (Continue on reverse side if necessary and identify by block number) The elevated deformation behavior of Zn-22% Al alloy was investigated, with special emphasis on the micromechanisms of deformation. Constant strain rate data on flow stress vs strain rate at different temperature and with specimens with different grain sizes were analyzed. From this analysis the constitutive equations for superplastic creep, dislocation-climb creep, cobble creep and Nabarro creep processes were established. Finally the results were depicted in the form of a three-dimensional deformation mechanism map with normalized parameters of grain size, temperature and stress as the coordinates.		

DD FORM 1473 1 JAN 73

Unclassified

SECURITY CLASSIFICATION OF THIS PAGE (When Data Entered)

82 08 26 021

FINAL SCIENTIFIC REPORT

GRANT - AFOSR-79-0069

Fundamental Investigations of Superplastic Forming Process

by

Professor Amiya K. Mukherjee
Division of Materials Science and Engineering
Department of Mechanical Engineering
Davis, California 95616

to

Dr. Alan Rosenstein
Air Force Office of Scientific Research
AFOSR/NE
Building 410
Bolling Air Force Base
Washington, D.C. 20332

March 1982

Accession For	
NTIS GRA&I	<input checked="checked" type="checkbox"/>
DTIC TAB	<input type="checkbox"/>
Unannounced	<input type="checkbox"/>
Justification	
By _____	
Distribution/ _____	
Availability Codes	
Dist	Avail and/or Special
A	



AIR FORCE OFFICE OF SCIENTIFIC RESEARCH (AFSC)
NOTICE OF TRANSMITTAL TO DTIC
This technical report has been reviewed and is
approved for public release IAW AFR 190-12.
Distribution is unlimited.
MATTHEW J. KERPER
Chief, Technical Information Division

CONTENTS

	<u>Page</u>
Section 1. Introduction	1
Section 2. High Temperature Diffusion Creep Controlled Behavior of ZN-22% Al Alloy Tested in Torsion	7
Section 3. Two and Three Dimensional Deformation Mechanism Maps for High Temperature Creep of Zn-22% Al Eutectoid Alloy	35
Section 4. List of Publications and Dissertations Completed	59
Section 5. List of Personnel Involved	60
Section 6. List of Coupling Activities with Other Groups Doing Related Research	61

SECTION 1.

INTRODUCTION

The phenomenon of micrograin superplasticity in which metals and alloys deform extensively at elevated temperatures under small stresses without risk of rupture is an area of much active study, at present. The superplastic forming process is being used in commercial metal forming operations, including fabrication of various parts of airframes. Often superplastic-forming combined with diffusion-bonding has enabled design engineers with remarkable flexibility in the designing of components for airframes, with significant saving in materials and cost of fabrication. The finished products usually have isotropic mechanical properties and remarkable surface finish, and parts can be formed to very close tolerances.

However, the superplastic-forming process has one major drawback. The forming rates are usually quite slow when compared with other hot working operations in metal forming technology. This factor has so far restricted the extensive adoption of superplastic forming operations. A sound theoretical understanding of the dependence of the superplastic strain rate on temperature, grain size, and flow stress will be of significant help in optimization of these process variables, so that the material can be deformed at the highest possible forming rates and still benefit from the exceptionally large, neck-free ductility associated with superplasticity.

There are three prerequisites for the manifestation of superplastic behavior:

- (a) A fine (in the range of a few microns) and reasonably stable grain size.
- (b) A deformation temperature equal to or in excess of half the melting point of the matrix in absolute degrees.
- (c) A strain-rate sensitivity value of approximately 0.5. The strain-rate sensitivity parameter "m" is defined by $\sigma = \dot{\epsilon}^m$ where σ is the flow stress and $\dot{\epsilon}$ is the strain rate.

In general, superplasticity belongs to a group of elevated temperature deformation mechanisms that are pertinent to fine-grained materials. These are Nabarro-Herring creep, coble creep, superplasticity, and dislocation creep. A short description of each of these mechanisms follows:

1. Nabarro-Herring Creep

It is observed only in very fine grained materials and at relatively high temperatures. It does not involve motion of dislocations. It occurs due to diffusion of atoms from the boundary of a grain where the average tensile stress is zero, to the boundary of the same grain where the average tensile stress is maximum. The result is elongation of the shape of the grains in the direction of tensile stress. In Nabarro-Herring creep:

$$\begin{aligned} \text{Strain rate} &\propto \frac{1}{(\text{grain size})^2} \\ &\propto (\text{stress})^1 \end{aligned}$$

The activation energy is that of volume diffusion because atoms diffuse through the grain interior.

2. Coble Creep

This mechanism is similar to Nabarro creep in that it is found only in fine-grained materials at elevated temperature. However, here the atoms move along the grain boundaries instead of through the grain interior, and the process requires less activation energy. Here, also, the grains get elongated in the direction of tensile stress, and dislocations are not involved.

In Coble creep:

$$\begin{aligned}\text{Strain rate} &\propto \frac{1}{(\text{grain size})^2} \\ &\propto (\text{stress})^1\end{aligned}$$

The activation energy is that for grain boundary diffusion which is about half of that for volume diffusion.

3. Superplasticity

This is also observed only in fine-grained material at elevated temperature. However, there are several important differences between this mechanism and Nabarro-Herring or Coble creep. In superplasticity one finds extensive evidence of grain boundary sliding and rotation of individual grains. The grains do not change their shape, i.e., they remain essentially equiaxed. And, as the name indicates, extensive amount of ductility is manifested (often in excess of 700-800% elongation) before failure can occur. Most of the theoretical models for this mechanism suggest that dislocations do move in the region close to the grain boundaries. As the grains slide past each other, stresses are set up at

grain boundary triple points. This produces a problem of accommodation at these triple points. The necessary accommodation is achieved by diffusional or plastic processes involving dislocations. The dislocations arrive at the boundary of the grains where they are annihilated during the accommodation process. The net result is that the grains in 3-dimension stay intact and voids do not open up easily at these triple point junctions of grain boundaries, thereby inhibiting premature failure.

In superplasticity:

$$\begin{aligned}\text{Strain rate} &\propto \frac{1}{(\text{grain size})^2} \\ &\propto (\text{stress})^2\end{aligned}$$

and the activation energy is that for grain boundary diffusion.

4. Dislocation Creep

This is the conventional micromechanism for regular creep. Most crystalline solids exhibit this type of creep at elevated temperatures. The existence of fine grains in the microstructure is not a necessary prerequisite. Single crystal specimens can also manifest such creep behavior. Weertman's dislocation-climb model is the standard model for this mechanism. The crept microstructure is often noted for presence of subgrains, and there is a prolonged transient stage (primary stage) in the creep curve (creep strain vs. time) plot for such mechanisms. Dislocations are produced by sources in parallel slip planes where they pile up. The lead dislocations from such pile-ups climb toward each other and annihilate one another, producing the steady state kinetics of the deformation process.

In dislocation creep:

Strain rate \propto (grain size)⁰, i.e. no dependence on grain size

Strain rate \propto (stress)⁵⁻¹⁰, depending on the material.

The activation energy of the process is that for volume diffusion. All materials, at sufficiently high stresses, will exhibit this creep mechanism.

Goals of AFOSR-Supported Research For UCD-College of Engineering Program:

The research program is designed to clarify the mechanical and microstructural properties in superplasticity. There are several specific areas of emphasis:

- a) Substructural investigation with critical attention paid to the structural modifications induced by superplastic flow.
- b) Delineation of ranges of operation of the superplastic process. This involves the application of thermodynamics, rate theory, constitutive equations for various high temperature deformation mechanisms with supportive evidence from optical scanning, and transmission electron metallography. The ultimate aim is to construct 3-dimensional "deformation-mechanism" diagrams (like phase diagrams) explicitly depicting the effect of temperature, stress, strain rate, and grain size for the operating field for superplasticity. Such diagrams will be extremely useful in optimizing the forming parameters in superplasticity. This group is the first to produce such 3-dimensional deformation mechanism diagrams in the United States.

- c) Study of the precise criteria for the transition from superplastic flow at intermediate stress and strain rates to dislocation creep at higher stresses and strain rates. Thorough investigation of the factors that may allow extension of the superplastic region to higher strain rates, for more economical operation.
- d) Study of the factors which lead to fracture during the superplastic process in terms of structural modification, cavitation, and geometrical instability.

It is anticipated that this study will provide, in the long run, improved guidelines for superplastic forming operations and for superplastic materials preparations.

We have used Zn-22% Al Eutectoid alloy as the model material for this work in order to determine the rate controlling mechanisms for elevated temperature deformation and also for the construction of three-dimensional deformation mechanism maps.

SECTION 2

HIGH-TEMPERATURE DIFFUSION-CONTROLLED CREEP BEHAVIOR OF
THE Zn-22% Al EUTECTOID ALLOY TESTED IN TORSIONAbstract

Torsion testing was carried out on Zn-22%Al eutectoid alloy and covered a range of strain-rates between $4.4 \times 10^{-5} \text{s}^{-1}$ and $4.2 \times 10^{-1} \text{s}^{-1}$, temperatures between 413°K and 533°K and grain sizes between $0.8 \times 10^{-4} \text{cm}$ and $3.5 \times 10^{-4} \text{cm}$. Within the range of strain-rates, temperatures and grain sizes investigated, four rate-controlling deformation mechanisms are found operative and are identified as Coble creep, Nabarro-Herring creep, superplastic creep and dislocation climb creep, respectively. The ranges of manifestation of each mechanism in terms of stress, strain-rate, temperature and grain size, are determined.

The four mechanisms are shown to relate to each other and new correlation form based on the newly proposed $\{AM\}$ parameter is developed. Furthermore, it is shown that for the high-temperature diffusion-controlled deformation mechanism, the value assumed by the $\{AM\}$ parameter, completely and uniquely identifies the rate-controlling deformation mechanism.

1. INTRODUCTION

Mukherjee, Bird and Dorn [1] have shown that for all high temperature diffusion-controlled deformation mechanisms the relation between the applied stress (τ) and the steady-state strain-rate ($\dot{\gamma}$) can be expressed by a dimensionless form:

$$\frac{\dot{\gamma} kT}{D G b} = A \left(\frac{b}{d} \right)^p \left(\frac{\tau}{G} \right)^n \quad (1)$$

where G is the shear modulus at the test temperature, D is the appropriate diffusivity (either for grain boundary or for lattice self-diffusion), b is the Burgers vector, d is the grain size, p is the grain size dependence of the strain-rate, n is the stress sensitivity coefficient and is equal to the reciprocal of the strain rate sensitivity coefficient ($n = 1/m$), and kT has the usual meaning of Boltzman's constant times absolute temperature.

D in Eq. (1) can be expressed as:

$$D = D_0 \exp \left(- \frac{Q}{RT} \right) \quad (2)$$

where D_0 is the diffusion coefficient, Q is the activation energy and R is the gas constant.

Combining Eqs. (1) and (2) we find that any high temperature diffusion-controlled mechanism is fully and uniquely defined by four parameters: Q , A , p and n . The nominal values of these parameters for the operative high temperature deformation mechanism are listed in Table I [2]. Thus, the experimentally determined values of Q , A , p and n for any material and condition can be directly compared with the values listed in Table I and the rate-controlling deformation mechanism, for any particular stress-temperature-grain size-strain-rate combination, can be unequivocally determined.

The Zn-22%Al eutectoid alloy is extremely well characterized and most suitable for basic studies in the field of superplastic deformation phenomenon. Although this alloy has been thoroughly investigated over the last fifteen years [3-21] its superplastic behavior is far from being fully understood. Not only different types of stress-strain-rate behavior have been reported for this alloy, but also the activation energies and grain size dependence of strain-rate reported, for the diffusional creep and Regions I and II, by the various investigators are in severe disagreement.

Table I - The nominal values of the parameters
in Eq. (1) for various high-temperature
diffusion-controlled deformation mechanisms [2]

Mechanism	A	n	p	D
Coble Creep	50	1	3	D_{gb}
Nabarro-Herring Creep	7	1	2	D_l
Harper-Dorn Creep	~ 10	1	0	D_l
Superplastic Creep	~200	2	2	D_{gb}
Dislocation Viscous Glide Creep	~ 3	3	0	D_l
Dislocation Climb Creep	$\sim 2 \times 10^6$	5	0	D

All these uncertainties about the exact mechanical and microstructural behavior of this alloy at elevated temperature make the task of identifying the rate-controlling deformation mechanism in the superplastic range extremely difficult. It is clear that in order to accomplish this task,

new data are required which will cover a large range of stress, temperature, grain size and strain-rates.

It is, therefore, the purpose of this investigation to provide additional mechanical and microstructural data and to try to correlate between the deformation mechanisms found operative within the range of stress-temperature-grain size investigated.

2. EXPERIMENTAL PROCEDURES

2.1 Material

The Zn-22% Al eutectoid alloy was supplied by Center for Technology, Kaiser Aluminum and Chemical Corporation, Pleasanton, CA 94566. The alloy was prepared by melting high purity 99.9999% Al and 99.9999% Zn into an air furnace. The melt was thoroughly mixed and degassed prior to being cast in a 24 in x 9 in x 3 1/4 in ingot. The chemical composition of the ingot as determined by spectrographic analysis was as follows: Zn = 77.47 - 77.54%; Si < 0.001%; Fe = 0.004%; Cu = 0.003%; Mn < 0.001%; Mg = 0.001%; Cr < 0.001%; Al = balance. Ni, Ti, Ga, and V and B were all reported as "Not Detectable". The chemical analysis was performed on samples from the ingot and duplicated on a sample from the plates following thermomechanical processing.

A layer of approximately 0.118 in was removed from each flat face of the ingot by machining to ensure that no contaminated material remained on the ingot.

The ingot was then homogenized at 710°F (376°C) for 48 hrs. A 60°F/hour heating rate was used followed by a fast furnace cool to 660°F (349°C) and stabilized for one hour at this temperature. Following the

stabilizing treatment, the ingot was rapidly transferred to the rolling machine and hot rolled immediately to a 1.003" nominal thickness plate followed by air cool.

The plate was heated at a rate of 50°F/hour to 710°F (376°C) and soaked for 16 hours followed by quenching into a brine solution at 2°F. When removed from the brine solution, the plate was extremely cold but when left standing at room temperature, the heat generated during the eutectoid decomposition made the plate too hot to handle.

In the as-received condition the grain size of the alloy was 0.8×10^{-4} cm (0.8 μ m) and specimens with additional grain sizes were prepared by statically annealing the material at $528 \pm 3^\circ\text{K}$ in a horizontal Ipsen furnace under a slightly positive argon pressure, for various lengths of time. The resulting grain sizes are shown in Table II. The kinetics of grain growth under static annealing conditions are shown in Fig. 1. It is evident from Fig. 1 that unreasonably long annealing times are required to obtain relatively large grain sizes. For example, to obtain a grain size of about 7.5×10^{-4} cm (7.5 μ m) annealing for almost two years is needed. Consequently, the largest grain size investigated was 3.5×10^{-4} cm (3.5 μ m) which was obtained after one week at the annealing temperature.

Table II - Initial grain sizes

Annealing Temperature [°K]	Annealing Time [hrs.]	Spatial Grain Size, Intercept x 1.74 [10 ⁻⁴ cm (μm)]
528 ± 2	0.0	0.8
	0.3	1.2
	2.0	1.7
	24.0	2.0
	42.0	2.9
	168.0	3.5

2.2 Mechanical testing

All the mechanical testing was carried out in torsion. The torsion test offers several advantages over the tensile test, namely:

- (a) Yields directly a shear stress - shear strain curve, which is more significant in characterizing the plastic behavior of the materials than a stress-strain curve determined in tension [22].
- (b) Tests are conducted at constant strain-rate.
- (c) Large strains can be achieved without necking.

A complete discussion of the advantages and disadvantages of the torsion test as compared to the tensile, compression and creep tests can be found elsewhere [22-24].

The torsion tests were carried out at Stanford University. Complete description of the torsion test apparatus at Stanford University was published elsewhere [24-26] and will not be repeated here. The test specimen, Fig. 2, was mounted on the test section of the apparatus having the liberty to move fully in the longitudinal direction. Thus, the

specimen was deformed essentially under pure torsion. The specimen was encapsulated in a quartz tube connected to a quenching apparatus. This enabled us to quench the specimen under pure torsion stresses at the instant the test was stopped. The heating to the test temperature was done into a split radiant furnace with a Chromel-Alumel thermo-couple attached to the specimen. At all the test temperatures used, the temperature variation was better than $\pm 2^\circ\text{K}$.

The torsion apparatus is capable of constant shear strain-rates between $5.4 \times 10^{-5}\text{s}^{-1}$ and $\sim 1.5 \times 10^2\text{s}^{-1}$, but around 10^1s^{-1} the recording apparatus started to lag behind, therefore creating an effective upper limit for the strain-rate at about 10^1s^{-1} . From the load-time recording the torsional strain (γ) and stress (τ) values were calculated using the following relations [26]:

$$= \frac{r}{\ell} \times (\text{rpm}) \times 2\pi \times t \quad (3)$$

$$= \frac{L \times a}{2 r^3} (M + N + 3) \quad (4)$$

where r = specimen's radius, ℓ = specimen's gage length, (rpm) = rotation per minute, t = testing time in minutes, L = load, a = the torque's arm (3 in), and M and N are, respectively, the slopes of $\log L$ versus $\log \dot{\gamma}$ (shear strain-rate) at constant γ and of $\log L$ versus $\log \gamma$ at constant $\dot{\gamma}$.

In order to avoid uncertainties due to the deformation induced micro-structural changes, all the mechanical data used in this investigation were collected at the maximum load in the load-time plot, in this case $N = 0$ (zero strain hardening). The M -values were taken from the $\log L$ versus $\log \dot{\gamma}$, at constant γ , plots. Most of the data presented in this paper were obtained from duplicate tests and, occasionally, triplicate tests were performed.

2.3 Metallographic techniques

Due to the difficulty in resolving the extremely fine grain sizes under the optical microscope, all the metallographic examinations were carried out on a scanning electron microscope using the back scattering technique [27]. Samples were mechanically polished on successive grit sizes silicon-carbide papers from 240 to 600 mesh. The final polishing was done, also mechanically, using diamond paste from 5 to 0.25 μm grit size.

The unetched specimens were examined in the scanning electron microscope. The pictures taken in the scanning electron microscope were analyzed on a Computerized Image Analyzer (Quantimet) [28,29], and the mean linear intercept (\bar{L}), mean form factor (F) and the total percentage area (A%) were quantitatively determined for α -rich and β -rich phases, respectively. The spatial grain size was calculated according to the relation [30]:

$$d = 1.74 \times \bar{L} \quad (5)$$

3. RESULTS

3.1 The shear stress - shear strain-rate relationship.

The shear stress - shear strain-rate relationship has a special significance in the study of high temperature deformation because it gives the investigator the first insight about the pertinent deformation mechanisms operative within the range of conditions investigated.

The shear stress vs. shear strain-rate datum points experimentally obtained at constant temperature and four different grain sizes are shown in Fig. 3 as a log - log plot.

It is clear from Fig. 3, that different shear stress - shear strain-rate relationships are obtained at different strain-rate values. At high strain-rates all the experimental points fall into a straight line with a slope of 0.2 ($n = 5.0$) regardless of the grain size value.

At intermediate strain-rates, the datum points fall on straight parallel lines, each line connecting the experimental datum points obtained with a single grain size value. The slope of these lines was found to be 0.5 ($n = 2.0$). The slope was clearly established for $1.7 \mu\text{m}$ grain size, whereas for other grain sizes only a few strain rates were investigated and the slopes are represented by broken lines. This procedure was used because it is now firmly established that $n = 1/m$ is independent of grain size and temperature within superplastic regime [9,10,16,17,21].

At the low strain-rates, the datum points are, again, arranged on straight lines, representing a single grain size value, but unlike the lines in the intermediate strain-rate range, not all of these lines are parallel, their slope depending upon the actual grain size value. For the grain sizes smaller and including $2 \mu\text{m}$, the slope of the lines is 0.8 ($n = 1.25$), whereas for grain sizes larger than $2 \mu\text{m}$ the slope is 1 ($n = 1$).

3.2 The grain size dependence of the shear stress

The shear stress dependence on the grain size is shown in Fig. 4, where the flow shear stress values versus the grain size were plotted at constant temperature and strain-rate, for two strain-rates corresponding to the intermediate and low strain-rate ranges, respectively, in Fig. 3.

The datum points obtained at $\dot{\gamma} = 1.88 \times 10^{-2} \text{s}^{-1}$ (intermediate range) can be connected by a straight line of slope 1.1. From Eq. (1) we can write for constant temperature and strain-rate:

$$\tau^n = \text{const.} (d)^p \quad (6)$$

and,

$$\log \tau = \log (\text{const.}) + \frac{p}{n} \log d \quad (6a)$$

Therefore, the slope of the line in Fig. 4 is equal to p/n . Since n was determined from the slope of the line in Fig. 3 and found equal to 2, we find that $p = 2.2$.

The experimental datum points obtained at $\dot{\gamma} = 2.5 \times 10^{-4} \text{ s}^{-1}$ are connected in Fig. 4 by two straight lines yielding slopes of 3.1 and 1.6 for grain sizes smaller or equal to $2 \mu\text{m}$ and larger than $2 \mu\text{m}$, respectively. Therefore, the p -values are 2.5 and 1.6 for $d \leq 2 \mu\text{m}$ and $d > 2 \mu\text{m}$, respectively.

3.3 Temperature effect

Fig. 5 shows the variation of the flow stress with the test temperature at constant strain-rate and grain size. At low temperatures (below 413°K) there is a linear dependence of the flow stress on temperature. At temperatures between 413°K and 533°K , the flow stress decreases logarithmically as the temperature increases. From the inspection of the Fig. 5 we may conclude that only at temperatures above 400°K is the deformation of this alloy diffusion controlled.

In order to determine the activation energies of the rate-controlling mechanism operative in the range of conditions under investigation in this work, the temperature dependence of the temperature corrected flow stress must be studied in all three strain-rate ranges shown in Fig. 3.

From Eq. (1) at constant strain-rate and grain size we can write:

$$\tau^{-n} G^{n-1} T = \text{const.} \exp \left(\frac{-Q}{RT} \right) \quad (7)$$

and

$$\log (\tau^{-n} G^{n-1} T) = \log (\text{const.}) + \left(\frac{-Q}{2.3R} \right) \left(\frac{1}{T} \right) \quad (7a)$$

when the left side of the Eq. (7a), i.e. the temperature compensated flow stress is plotted versus $(1/T)$, the slope of the

lines is equal to $\frac{-Q}{2.3R}$. Thus,

$$Q = -2.3 R \times (\text{slope}) \quad (8)$$

To construct plots $\log (\tau^{-n} G^{n-1} T)$ versus $(1/T)$, the variation of G with temperature must be known. The shear modulus, G , for the alloy is given by:

$$G = N_{Al} G_{Al} + N_{Zn} G_{Zn} \quad (9)$$

where N_{Al} and N_{Zn} are the atomic fractions of aluminum and zinc, respectively. The individual shear modulus G_{Al} and G_{Zn} can be estimated as:

$$G = G_0 - \Delta G T \quad (10)$$

where G_0 is the value of the shear modulus at 0°K and ΔG is the variation of the shear modulus per degree Kelvin.

Combining the Eq. (9) and (10) we obtain:

$$G_{\text{alloy}} = (N_{Al} G_0 Al + N_{Zn} G_0 Zn) - (N_{Al} \Delta G_{Al} + N_{Zn} \Delta G_{Zn}) T \quad (11)$$

Taking $N_{Al} = 0.4$, $N_{Zn} = 0.6$, $G_0 Al = 3.02 \times 10^{11}$ dynes/cm² [31], $G_0 Zn = 5.98 \times 10^{11}$ dynes/cm² [32], $\Delta G_{Al} = 1.6 \times 10^8$ dynes/cm² [31] and, $\Delta G_{Zn} = 3.37 \times 10^8$ dynes/cm² [32] and substituting in Eq. (11), we obtain the shear modulus for the alloy as:

$$G = (4.796 \times 10^{11} - 2.662 \times 10^8 T) \frac{\text{dynes}}{\text{cm}^2} \quad (12)$$

Fig. 6 shows such a plot for the high strain-rates range. The slope of the line yields an activation energy of 28,300 cal/mole. This value is somewhere between the lattice self-diffusion activation energies in pure aluminum, $Q = 34,200$ cal/mole [33,34] and in pure zinc, $Q = 21,800$ cal/mole and 24,300 cal/mole for diffusion parallel and perpendicular to the hexagonal axis, respectively [35].

For the intermediate strain-rates, the semilogarithmic plot of the temperature compensated flow stress versus reciprocal of temperature, Fig. 7, yields an activation energy of 13,100 cal/mole. This value is comparable with the activation energy for grain-boundary diffusion in pure zinc, 14,500 cal/mole [36].

For the low strain-rate range, $\log (\tau^{-n} G^{n-1} T)$ vs $(1/T)$ plot was constructed for two grain sizes, $d = 1.7 \mu\text{m}$ and $d = 3.5 \mu\text{m}$, Fig. 8, because the previous results (paragraph 2.2 and 2.3) indicated different behavior for specimens having grain sizes smaller and larger than $2 \mu\text{m}$, respectively.

For the $1.7 \mu\text{m}$ grain size, the datum points fall closely onto a straight line, which yields a slope of 10,200 cal/mole. On the other hand, the data for the larger grain size yields two different values of the activation energy depending upon the temperature range. At temperatures higher than about 500°K , the activation energy was identical to that obtained for high strain-rate range, 28,300 cal/mole. At temperatures below 500°K , the slope of the line connecting between the experimental points yields an activation energy identical to that obtained for the $1.7 \mu\text{m}$ grain size in this strain-rate range.

3.4 Determination of the parameter A in Eq. (1).

According to the Eq. (1), the parameter A is given by:

$$\log A = \log \frac{\dot{\gamma} k T}{D_{gb}} \left(\frac{d}{b}\right)^p - n \log \left(\frac{\tau}{G}\right) \quad (13)$$

or the numerical value of the $\log A$ will be equal with the numerical value of the first term in the right side of the Eq. 13 when $\tau/G = 10^\circ$. Consequently, in a log-log plot of $\frac{\dot{\gamma} k T}{D_{gb}} \left(\frac{d}{b}\right)^p$ vs. $\frac{\tau}{G}$, the A-value will correspond to the intercept of the straight line connecting between the experimental datum points with the vertical $\tau/G = 10^\circ$. Such a plot is shown in Fig. 9. To construct this plot, b was taken as 2.8×10^{-8} cm and D_0 as $1.0 \text{ cm}^2/\text{s}$. Furthermore, in order to present all the experimental data on one plot, in the first term in the right side of the Eq. (13), D was assumed identical to D_{gb} and the whole term was multiplied by $(D_{gb}/d_\ell)^\alpha$. For the datum points from the regions where an activation energy close to that for grain-boundary diffusion was obtained α is equal to zero, and for those experimental points associated with an activation energy close to that for lattice self-diffusion, α is unity.

The A-values obtained from Fig. 9 are listed in Table III.

Table III - Summary of the experimental values for the parameters in Eq. (1).

Strain Rate Range	Grain size	A	p	n	Q [cal/mole]
low	$\leq 2 \mu\text{m}$	106	2.5	1.25	10,200
low	$> 2 \mu\text{m}$	80	1.6	1	28,300
intermediate	all	80	2.2	2	13,100
high	all	5.7×10^6	0	5	28,300

4. DISCUSSION

In this section we will try to find answers at two major questions which are vital to our understanding of the high temperature deformation behavior of materials, superplastic behavior included. The first question is: "Which are the rate-controlling deformation mechanisms operative in the space stress-strain-rate-temperature-grain size investigated?". The second question can be formulated as: "If more than one single rate-controlling deformation mechanism is found operative, do they correlate?".

4.1 The rate-controlling deformation mechanisms

The results of the mechanical tests presented in Section 3 clearly indicate that four different mechanisms operate within the range of stress-strain-rate-temperature-grain size investigated in this work. At

high strain-rates, a unique mechanism seems to be rate controlling for all the temperatures and grain sizes investigated. The same is true for the intermediate strain-rate region. At low strain-rates, two deformation mechanisms are found operative depending upon the grain size. Each of these mechanisms will now be considered separately.

a. High strain-rate region (Region III)

The constitutive equation for the rate-controlling mechanism in this region can be written in terms of Eq. (1) as:

$$\frac{\dot{\gamma} kT}{D_0 G b} = 5.7 \times 10^6 \left(\frac{T}{G}\right)^5 \exp\left(\frac{-28,300}{RT}\right) \quad (14)$$

The values of the parameters A, Q, p and n in Eq. (14) suggest that the rate-controlling deformation mechanism is the climb of dislocations [1,2]. For Zn-22% Al eutectoid alloy, a similar conclusion was reached by Vaydia et al [10], Misro and Mukherjee [16] and Mohamed and Langdon [17,18].

A more complete analysis of this mechanism is complicated by the duplex nature of the alloy. The Al-rich phase (α -phase) has an F.C.C. crystal structure and the width of the stacking-fault energy might affect the dislocation climb mechanism in several ways. First, it seems that an increase in the stacking fault energy will increase the creep rate, [37,38]. This was interpreted by Barret and Sherby [39] as an increase in the value of parameter A (Eq. (1)) with the increase in the stacking fault energy. This seems reasonable since the value of the parameter A includes all the microstructural details pertinent to the creep mechanism under consideration except the effect of the grain size. However, Mukherjee and coworkers [1] challenged this interpretation, showing that Barret and Sherby's approach assumes that n will be constant for all FCC metals.

They proposed as an alternative possibility, that A will remain constant for all FCC metals and the n -value will decrease as the stacking fault energy will increase. The net result will be, again, an increase in the creep rate. This assumption is substantiated by a reanalysis of the data published in the literature [2] which clearly indicated that n increases systematically when the stacking-fault energy decreases. The uncertainty regarding the exact stacking-fault energy value for Al-rich phase and its effect on the dislocation climb mechanism might induce some numerical error in the value of A or n , or both, in Eq. (14).

The second phase present in the Zn-22% Al eutectoid alloy, is the Zn-rich (β) phase. The crystallographic structure of this phase is HCP and its homologous temperature, T_H ($T_H = T/T_M$, where T is the actual temperature and T_M is the melting point of the metal, both given in °K) is higher within the range investigated than the homologous temperature of the α -phase ($T_{H\beta} = 0.6 - 0.77$ as compared to $T_{H\alpha} = 0.44 - 0.57$). The creep of HCP metals at temperatures greater than $T_H = 0.6 - 0.7$ appears to be governed by a separate mechanism which is characterized by a distinctly higher activation energy [2]. This mechanism is as yet unidentified. The activation energy for this unidentified mechanism is given approximately by $27R T_H$ [2], where R is the gas constant. For Zn this will lead to an activation energy of about 37.4 kcal/mole. Since the activation energy for lattice self-diffusion in pure Al is approximately 34.2 kcal/mole [33,34], then in the presence of the unidentified mechanism, the activation energy for alloy might be expected to be anywhere between 34 and 37 kcal/mole. However, the experimental activation energy was found equal to 28.3 kcal/mole, which is between the

activation energies for lattice self-diffusion in pure Al and Zn, respectively. This value of the experimental activation energy indicates that the high-temperature unidentified deformation mechanism was not operative in the β -phase of this alloy and probably the normal dislocation creep took place. The rate equation for dislocation creep in the HCP metals is similar to that for low stacking-fault energy FCC metals.

Therefore, we might conclude that within the limitation of the foregoing discussion the rate-controlling and dominant mechanism in the Region III is the climb of dislocations.

b. Intermediate strain-rate region (Region II)

The rate equation for the experimental data obtained in this region is given by:

$$\frac{\dot{\gamma}kT}{D_0Gb} = 80 \left(\frac{b}{d}\right)^{2.2} \left(\frac{T}{G}\right)^2 \exp\left(\frac{-13,100}{RT}\right) \quad (15)$$

Eq. (15) compares extremely well with those found to describe the superplastic creep behavior by other investigators [9,10,16,17,21]. The experimental activation energy indicates that the creep in this region is governed by the grain boundary diffusivity and the stress sensitivity (n) and grain size dependence of strain-rate (p) coefficients have values characteristic of superplasticity (see Table I). The only real discrepancy among the published results for this alloy in Region II is the value of A (Eq. (1)). Whereas most of the investigations [9,10,16] report an A -value of 150 ± 100 , others obtained A -values greater by one to four orders of magnitude [19,21]. An A -value of about 150 ± 100 is in good agreement with models for superplastic flow which predict that grain boundary sliding is the dominant mechanism while the rate is controlled by dislocation motion

which accommodates the sliding at triple points [9,40-42]. However, all these models calculate the A-value only from geometrical considerations, without including any of the subtle microstructural details which are by definition incorporated into it [1,2]. Therefore, in these models A appears as a universal constant regardless of the alloy, condition, etc.

c. Low strain-rate region (Region I) - small grain sizes.

The rate equation for this region is given by:

$$\frac{\dot{\gamma} kT}{D_0 G b} = 106 \left(\frac{b}{d}\right)^{2.5} \left(\frac{\tau}{G}\right)^{1.25} \exp\left(\frac{-10,200}{RT}\right) \quad (16)$$

Eq. (16) indicates that the rate-controlling deformation mechanism at low strain-rate and small grain size region is the diffusion of the vacancies along the grain boundaries, i.e., Coble creep [43]. The original equation developed on theoretical grounds [43], predicted an A-value equal to $150/\pi = 48$, which is only half of the experimental value obtained in this work. But as pointed out by Coble in the original publication [43], the assumption made to develop the rate equation, e.g., that the generation and annihilation rates for vacancies are uniform and equal, may not be valid. In the cases where the rates are non-uniform and unequal, the predicted rate would differ by a numerical factor, without affecting the n and p values.

The deviation of the grain size dependence of the strain-rate coefficient from the theoretical value (2.5 instead of 3) can be explained when we consider that the diffusional creep rate is a function of the diffusion path length and thus varies with grain shape as well as grain size. Raj and Ashby [44] treated the case when the grain aspect ratio deviates from the equiaxed condition (aspect ratio equal to unity) and

calculated that when the aspect ratio is much higher than unity the strain-rate dependence on grain size changes from $\dot{\gamma} \propto 1/d^3$ toward $\dot{\gamma} \propto 1/d^2$. For our alloy, the grain aspect ratio at the beginning of deformation varied between 1.6 and 1.8 and the experimental strain-rate dependence on grain size was found as $\dot{\gamma} \propto 1/d^{2.5}$.

d. Low strain-rate region (Region I) - large grain sizes

The rate equation for this region is given by:

$$\frac{\dot{\gamma} kT}{D_0 G b} = 80 \left(\frac{b}{d}\right)^{1.6} \left(\frac{\tau}{G}\right)^1 \exp\left(-\frac{28,300}{RT}\right) \quad (17)$$

The Eq. (17) describes the Nabarro-Herring diffusional creep [45,46], i.e., the diffusion of vacancies through the lattice from a boundary under normal tensile stress to a boundary under normal compressive stress and displacement of matter in the opposite direction. The slight deviations of the experimentally determined A and p-values from the theoretically predicted values, can be discussed and explained in the same manner as was done in Section 4.1 c.

4.2 Correlation of the operative creep mechanisms

In the preceding section of this paper, four individual diffusion-controlled creep mechanisms were identified as being operative with the stress-strain-rate-temperature-grain size range investigated and the applicable rate equations for each mechanism were developed. In the present section the way in which these mechanisms are related to one another will be considered.

The steady-state creep rates, as given by $\dot{\gamma} kT/DGb$ versus τ/G , for all four mechanisms identified in Section 4.1, are shown in Fig. 10. To permit ready comparison between the mechanisms controlled by lattice

diffusion and those controlled by grain boundary diffusion, the ordinate in Fig. 59 was given as $\frac{\dot{\gamma} k T}{D_{gb} G b} \frac{D_{gb}^{\alpha}}{D_{\ell}^{\alpha}}$, where α is zero for the grain boundary diffusion controlled mechanisms (i.e. Coble and superplastic creep) and unity for the lattice diffusion-controlled mechanisms (i.e. Nabarro-Herring and dislocation climb creep).

In Fig. 10, all the experimental datum points within one mechanism and representing one grain size value fall onto a single, straight line of a slope equal to the appropriate n -value for the mechanism under consideration and with an intercept equal to $A(b/d)^p$. The datum points representing the various grain sizes investigated fall on parallel, straight lines. Of special interest is the behavior at low strain-rates where two mechanisms were found operative within the same range of strain-rates. At low grain sizes Coble creep is operative and at large grain sizes Nabarro-Herring takes over. For the same applied stress, the Coble creep is the fastest of the two. Moreover, for the same grain size (3.5 μm) both Coble and Nabarro-Herring creep can be operative depending upon the test temperature.

Another type of correlation, based on the correlation proposed by Arieli and Rosen (47) for the superplastic creep and extended to include all the high temperature diffusion-controlled creep mechanisms, will be presented here.

If we rewrite Eq. (1) as,

$$\frac{\dot{\gamma} k T}{D G b} \left(\frac{d}{b}\right)^p = A \left(\frac{\tau}{G}\right)^n \quad (1a)$$

and assume that for a given creep mechanism the parameters p and n have constant, universal values (Table I), then the left side of the Eq. (1a) will give the limiting values of the range of conditions, for any combination of strain-rates, temperatures and grain sizes, over which each mechanism predominates.

Fig. 11 shows that all the experimental datum points obtained over a strain-rate range of about five orders of magnitude (10^{-5} to 10^0), temperatures from 413°K to 533°K and grain sizes between 0.8 μm and 3.5 μm , fall onto a single, straight line of the slope 1 when plotted as $\frac{\dot{\gamma}kT}{DGB} \left(\frac{d}{b}\right)^p$ versus $A \left(\frac{T}{G}\right)^n$. The straight line in Fig. 11 is divided in four distinct regions, each one representing a unique creep mechanism and defined by the values taken by the left side of the Eq. (1a).

The plot shown in Fig. 11 can be further extended to correlate not only among the creep mechanisms operative for a given alloy but also for different alloys. To do that, we have only to select standard values for $D = D_S$ (either grain boundary or lattice, as appropriate) $G = G_S$, $b = b_S$ and to multiply the left side of the Eq. (1a) by the ratio $\frac{D_S G_S b_S}{D_M G_M b_M}$ where D_M , G_M , and b_M are the appropriate values for the material under consideration. The parameter A on the right side of Eq. (1a) will vary not only from one alloy to another, but for the same alloy with different microstructural conditions. However, the variation of the parameter A will only translate the line in Fig. 11 to the right or the left, without changing the value of the left side of Eq. (1a).

Therefore, we propose a parameter $\{AM\}$ given by:

$$\{AM\} \text{ parameter} = \frac{\dot{\gamma}kT}{D_S G_S b_S} \left(\frac{d}{b}\right)^p \quad (18)$$

which uniquely defines the ranges of operation of each high temperature diffusion-controlled creep mechanism for a given alloy and can be used to correlate among different alloys when the experimental datum points are plotted as:

$$\{AM\} \text{ parameter} \times \frac{D_s G_s b_s}{D_M G_M b_M} \text{ vs } A \left(\frac{T}{G}\right)^n$$

Eventual applications of this parameter might include experimental work planning, prediction of the operative creep mechanisms in high temperature environment service of various alloys, alloy selection for creep service, etc.

5. SUMMARY AND CONCLUSIONS

The results of the experimental investigation present in this report show that four distinct rate-controlling creep mechanisms are operative within the range of stress-strain-rate-temperature-grain size investigated, i.e. Coble creep, Nabarro-Herring creep, superplastic creep and, dislocation climb creep, respectively.

The four creep mechanisms mentioned above are related to each other, and each one of them is rate-controlling over a definite range of stress-strain-rate-temperature-grain size. The range within which one mechanism is rate-controlling can be completely and uniquely defined by a new parameter introduced by this paper, the {AM} parameter. The {AM} parameter was shown to be a universal parameter, which can be used to correlate among the high temperature creep mechanisms operative for a single alloy as well as to compare the high temperature creep behavior of different alloys.

Acknowledgements

The authors acknowledge the help provided by Drs. T. R. Pritchett, R. C. Dorward and W. R. Mohondro, Center for Technology, Kaiser Aluminum and Chemical Corporation, who kindly supplied the alloy used in this investigation. The help provided by Drs. O. Sherby, J. Wedworth and Mr. T. Oyama, Department of Materials Science and Engineering, Stanford University, in allowing us to use their torsion apparatus is warmly acknowledged. Last, but not the least, the authors thank their colleagues B. McLean and R. Logan for the help with the experimental part of this program.

This work was carried out under an AFOSR Grant No. 79-0069.

References

1. A. K. Mukherjee, J. E. Bird and J. E. Dorn, Trans. ASM, 62, 155, (1969).
2. J. E. Bird, A. K. Mukherjee and J. E. Dorn, in "Quantitative Relation Between Properties and Microstructure", eds. D. G. Brandon and A. Rosen, p. 255, Israel Univ. Press, Jerusalem, (1969).
3. C. M. Packer and O. D. Sherby, Trans. ASM, 60, 21, (1967).
4. P. Chaudhari, Acta. Met., 15, 1777, (1967).
5. T. H. Alden and H. W. Shadler, TMS-AIME, 242, 825, (1968).
6. D. L. Holt, TMS-AIME, 242, 25, (1968).
7. R. H. Johnson, C. M. Packer, L. Anderson and O. D. Sherby, Phil. Mag., 18, 1309, (1968).
8. K. Nuttal and R. B. Nicholson, Phil. Mag., 17, 1087, (1968).
9. A. Ball and M. M. Hutchinson, Met. Sci. J., 3, 1, (1969).
10. M. L. Vaidya, K. L. Murty and J. E. Dorn, Acta. Met., 21, 1615, (1973).
11. R. B. Nicholson, in "Electron Microscopy and Structure of Materials", ed. G. Thomas, p. 689, University of California Press, Berkeley (1972).
12. O. A. Kaybyshev and I. V. Kazachov, Fiz. Metal. Metalloved., 34, (2), 396, (1972).
13. O. A. Kaybyshev, I. V. Kazachkov and V. M. Rozenberg, Fiz. Metal. Metalloved., 36, (6), 1235, (1973).
14. K. N. Melton and J. W. Edington, Scripta. Met., 8, 1141, (1974).
15. H. Naziri, R. Pearce, M. Henderson-Brown and K. F. Hale, Acta. Met., 23, 489, (1975).

16. S. C. Misro and A. K. Mukherjee, in "Rate Processes in Plastic Deformation", eds. J. C. M. Li and A. K. Mukherjee, p. 434, ASM, Metals Park, Ohio, (1975).
17. F. A. Mohamed and T. G. Langdon, Acta. Met., 23, 117, (1975).
18. F. A. Mohamed, S. A. Shei and T. G. Langdon, Acta. Met., 23, 1443, (1975).
19. O. A. Kaybyshev, I. V. Kazachov and S. Ya. Salikhov, Acta. Met., 26, 1887, (1978).
20. O. A. Kaybyshev, B. V. Rodionov and R. Z. Valiev, Acta. Met., 26, 1877, (1978).
21. A. Arieli, A. Yu and A. K. Mukherjee, Met. Trans., in print.
22. G. E. Dieter, Mechanical Metallurgy, McGraw-Hill, Kogakusha Ltd., Tokyo, (1961).
23. H. J. McQueen and J. J. Jonas, in "Metal Forming: Interrelation Between Theory and Practice", ed. A. L. Hoffmann, p. 393, Plenum, New York, (1971).
24. J. L. Robbins, H. Wagenaar, O. C. Shepard and O. D. Sherby, 6th Technical Report to the American Iron and Steel Institute, DMS Report no. 65-38, Stanford University, Stanford, CA, (1965).
25. J. L. Robbins, O. C. Shepard and O. D. Sherby, Trans. ASM, 60, 205, (1967).
26. J. L. Robbins, H. Wagenaar, O. C. Shepard and O. D. Sherby, J. of Mater., 2, (2), 271, (1967).
27. V. A. Phillips, "Modern Metallographic Techniques and Their Applications", Wiley-Interscience, New York, (1971).
28. H. F. Fischmeister, in "Quantitative Microscopy", eds. R. T. Dittoff and F. N. Rhines, p. 336, McGraw-Hill Book Co., New York, (1968).

29. G. A. Moore, L. L. Wyman and M. M. Joseph, *Ibid.*, p. 381.
30. F. Schuckher, *Ibid.*, p. 201.
31. P. M. Sutton, *Phy. Rev.*, 91, 816, (1953).
32. G. A. Alers and J. R. Neighbor, *J. Phy. Chem. Solids*, 7, 58, (1958).
33. T. S. Lundy and J. F. Murdock, *J. Appl. Phys.*, 33, 1671, (1962).
34. M. Beyeler and Y. Adda, *J. de Phys.*, 29, 345, (1968).
35. G. A. Shiru, E. S. Wajda and M. B. Huntington, *Acta. Met.*, 1, 513, (1953).
36. E. S. Wajda, *Acta. Met.*, 2, 184, (1954).
37. P. Feltham, in "Structural Processes in Creep", p. 82, Iron and Steel Institute, London, (1961).
38. D. McLean, *Met. Reviews*, 7, 481, (1962).
39. C. R. Barrett and O. D. Sherby, *TMS-AIME*, 230, 1322, (1964).
40. R. C. Gifkins, *Met. Trans.*, 7A, 1225, (1976).
41. A. K. Mukherjee, *Mat. Sci. Engr.*, 8, 83, (1971).
42. A. K. Mukherjee, in "Proc. Bolton-Landing Conf. Grain Boundaries 4th", p. 93, (1975).
43. R. L. Coble, *J. Appl. Physics*, 34, (6), 1679, (1963).
44. R. Raj and M. F. Ashby, *Met. Trans.*, 2, 1113, (1971).
45. F. R. N. Nabarro, *Report of Conference on Strength of Solids*, Phys. Soc. London, (1948).
46. C. J. Herring, *J. Appl. Phys.*, 21, 437, (1950).
47. A. Arieli and A. Rosen, *Met. Trans.*, 8A, 1591, (1977).

List of Figures

- Fig. 1 Grain size versus static annealing time.
- Fig. 2 Torsion test specimen's dimensions.
- Fig. 3 Log-log plot of the shear stress versus shear strain-rate for various grain sizes at 503°K.
- Fig. 4 Log-log plot of the shear stress versus grain size for two strain-rates at 503°K.
- Fig. 5 The variation of the flow stress with the temperature.
- Fig. 6 Temperature compensated flow stress versus the reciprocal of temperature (high strain-rate region).
- Fig. 7 Temperature compensated flow stress versus the reciprocal of temperature (intermediate strain-rate region).
- Fig. 8 Temperature compensated flow stress versus the reciprocal of temperature (low strain-rate region).
- Fig. 9 Log-log plot of $\left[\frac{\dot{\gamma} k T}{D G B} \left(\frac{d}{B} \right)^p \right]$ vs. (τ/G) .
- Fig. 10 Correlation of the deformation mechanisms as $\log \left[\frac{\dot{\gamma} k T}{D G B} \right]$ versus $\log (\tau/G)$.
- Fig. 11 Correlation of the deformation mechanisms as $\log [\{AM\} \text{ parameter}]$ versus $\log [A(\tau/G)^n]$.

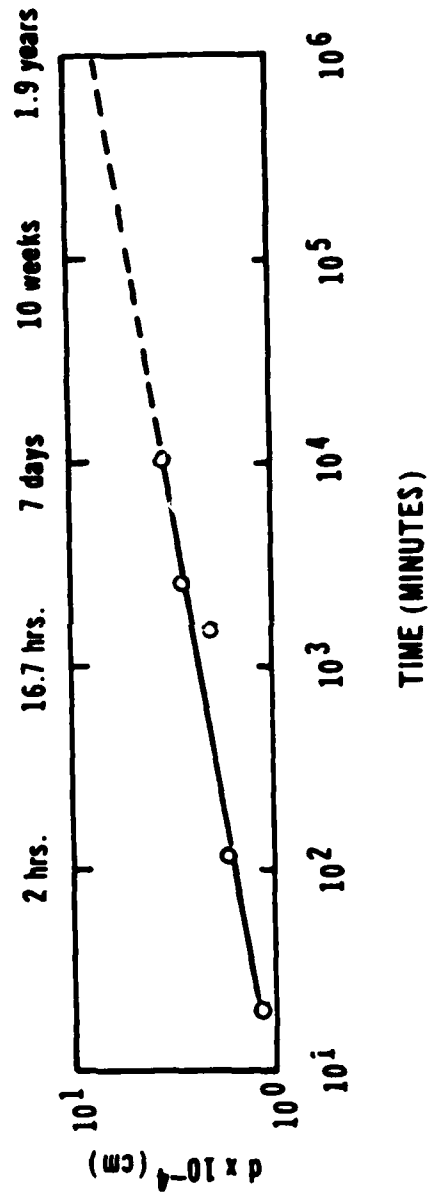


Fig. 1 Grain size versus static annealing time.

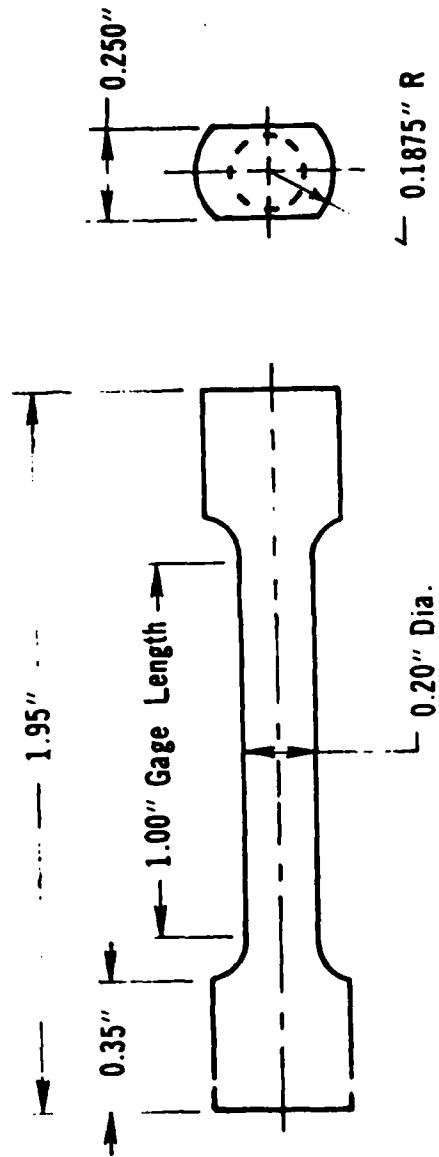


Fig. 2 Torsion test specimen's dimensions.

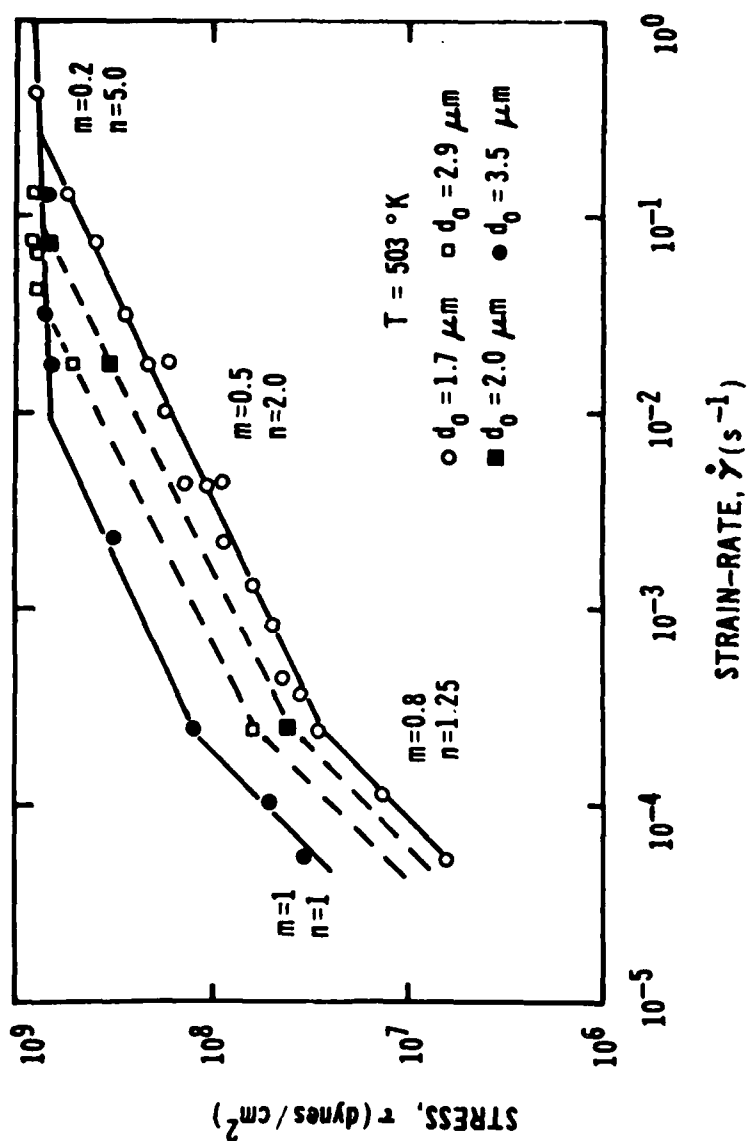


Fig. 3 Log-log plot of the shear stress versus shear strain-rate for various grain sizes at 503°K .

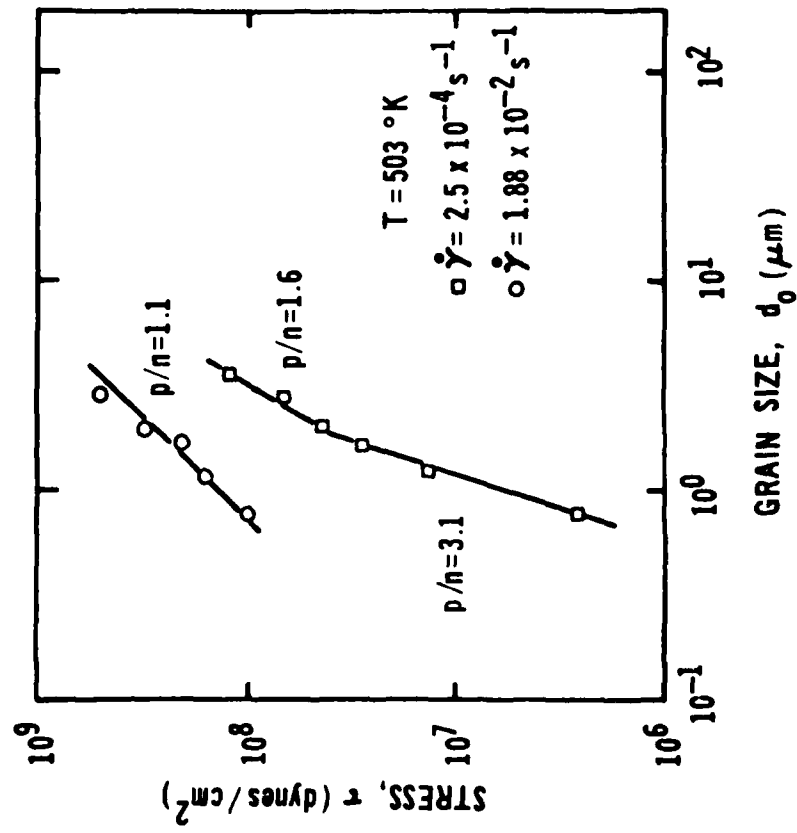


Fig. 4 Log-log plot of the shear stress versus grain size for two strain-rates at 503°K .

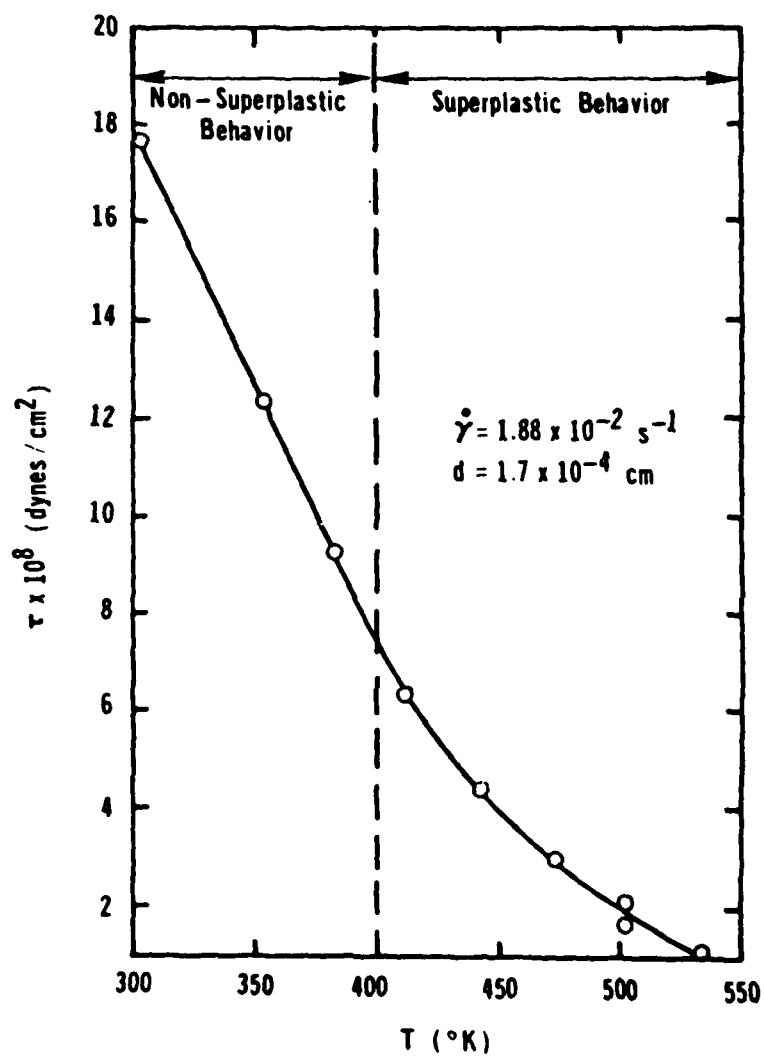


Fig. 5 The variation of the flow stress with the temperature.

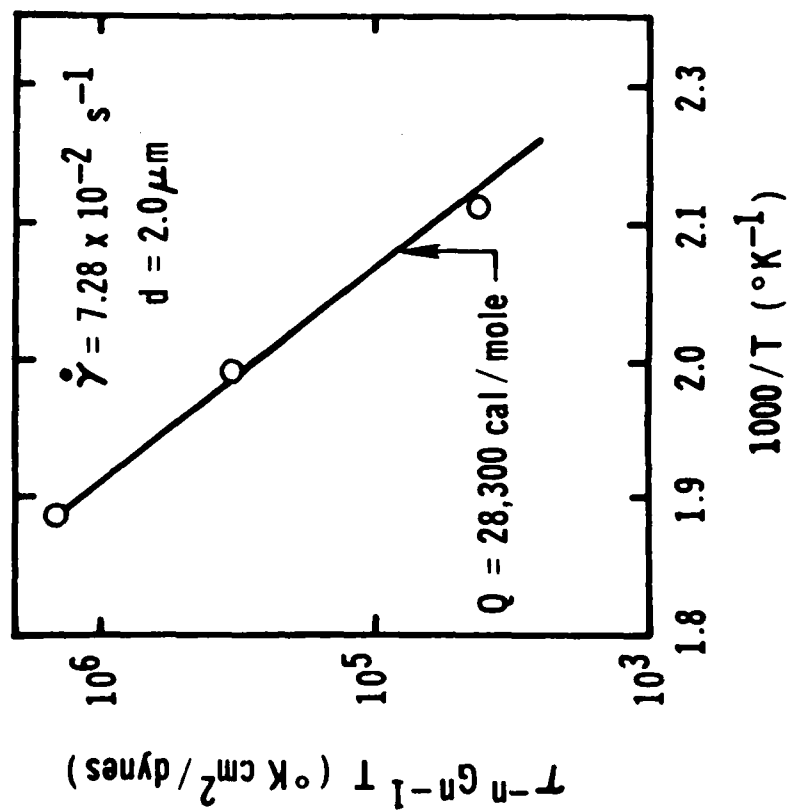


Fig. 6 Temperature compensated flow stress versus the reciprocal of temperature (high strain-rate region).

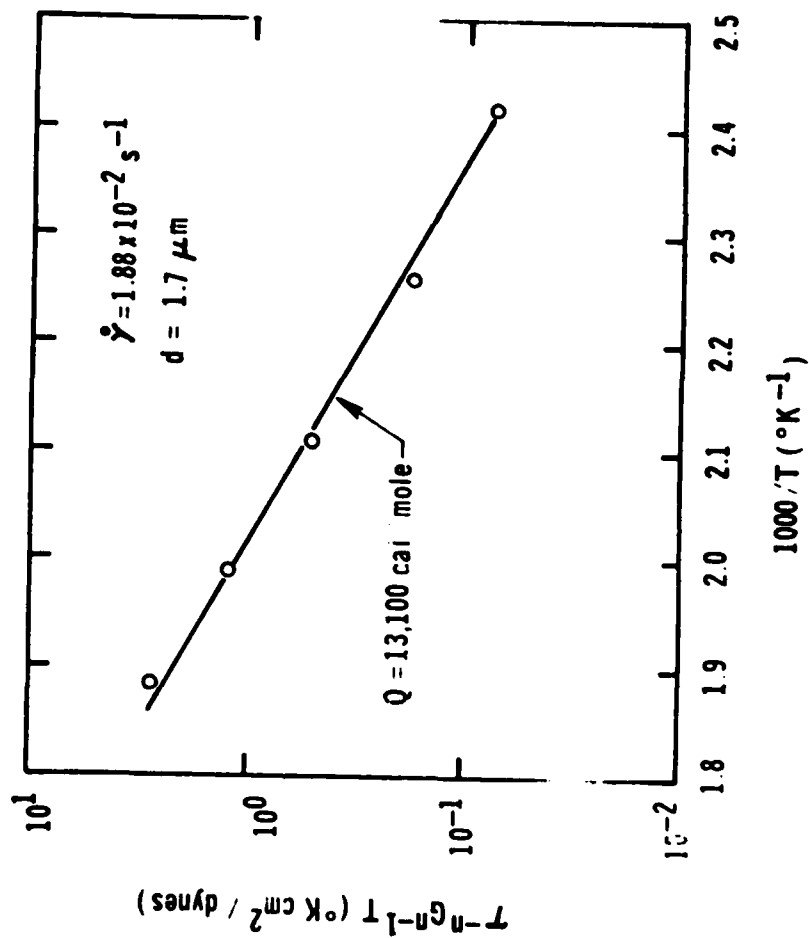


Fig. 7 Temperature compensated flow stress versus the reciprocal of temperature (intermediate strain-rate region).

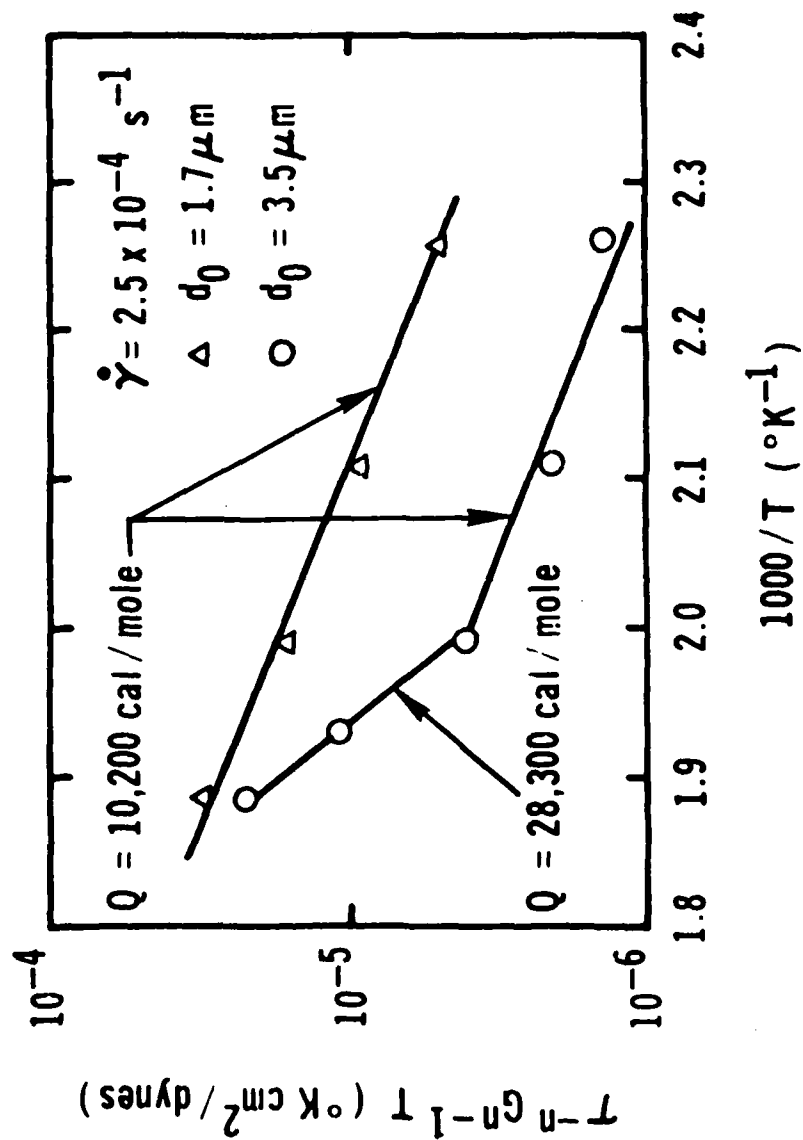


Fig. 8 Temperature compensated flow stress versus the reciprocal of temperature (low strain-rate region).

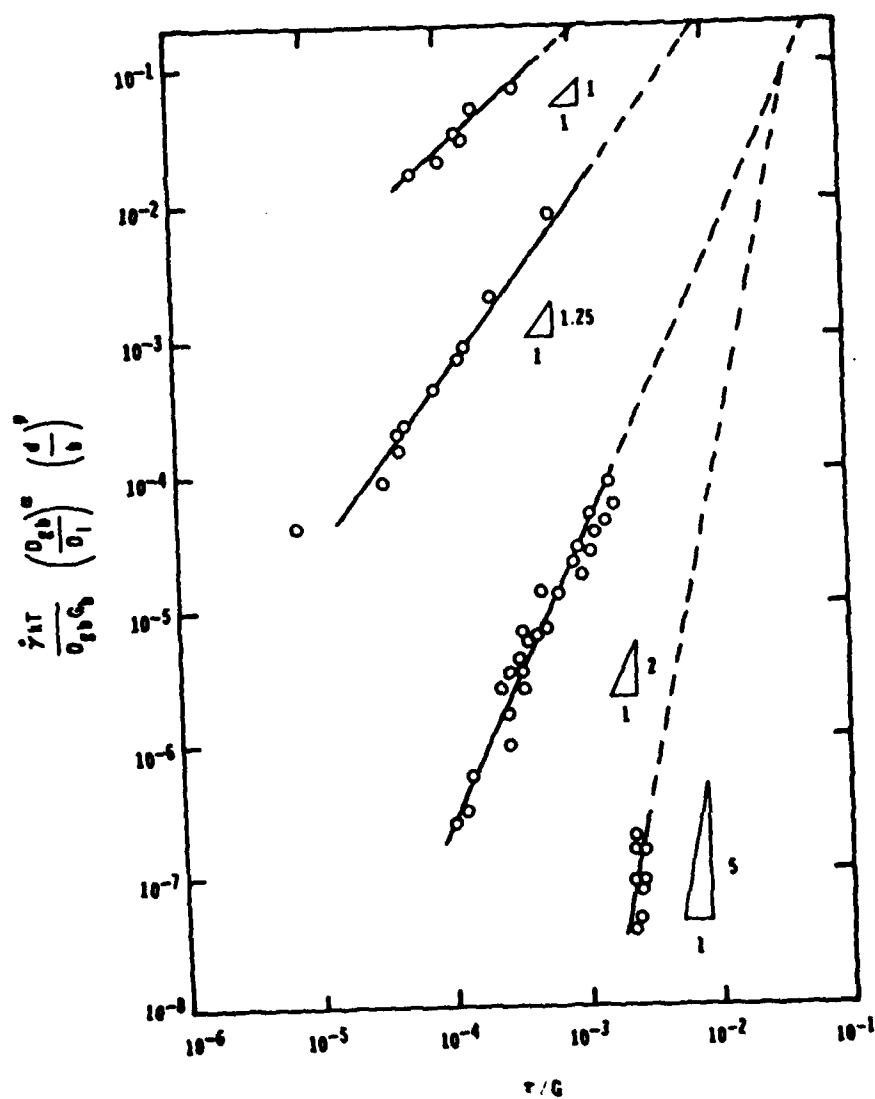


Fig. 9 Log-log plot of $\left(\frac{\gamma kT}{0.25 G_0} \right) \left(\frac{d}{b} \right)^p$ vs. (τ/G) .

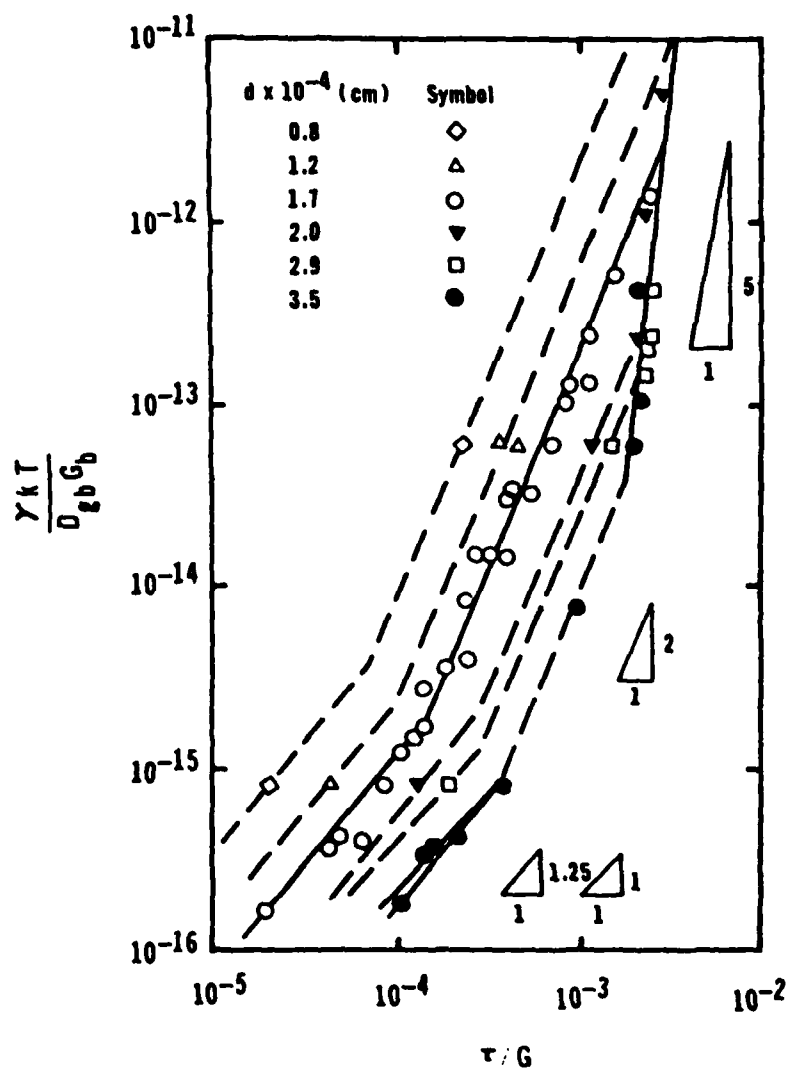


Fig. 10 Correlation of the deformation mechanisms as $\log \left(\frac{\dot{\gamma} k T}{D_{GB} G_b} \right)$ versus $\log (\tau/G)$.

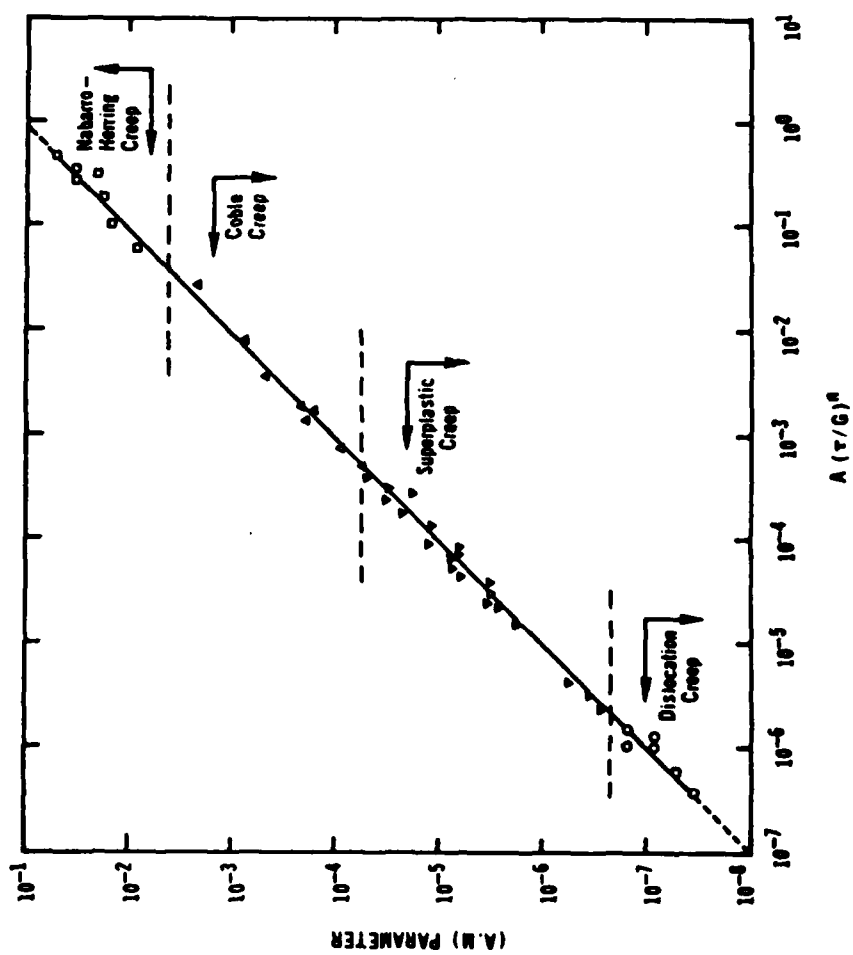


Fig. 11 Correlation of the deformation mechanisms as $\log [AM \text{ parameter}]$ versus $\log [A(\tau/G)^n]$.

SECTION 3

TWO- AND THREE-DIMENSIONAL DEFORMATION MECHANISM
MAPS FOR HIGH TEMPERATURE CREEP
OF Zn-22%Al EUTECTOID ALLOY

Adi Arieli and Amiya K. Mukherjee

Division of Materials Science and Engineering
Department of Mechanical Engineering
University of California
Davis, CA 95616

ABSTRACT

This paper analyzes the relations among the rate-controlling deformation mechanisms found operative for Zn-22% Al eutectoid alloy in terms of two-dimensional deformation maps that are in current use. Although useful in their simplicity, the two-dimensional deformation mechanism maps have one main drawback, i.e., their lack of generality. One must construct many maps, even for limited ranges of stress, temperature, and grain size in order to obtain the overall picture. In order to overcome this limitation, a new type of deformation mechanism map, a three-dimensional one, is developed and introduced in this paper. Possible application of this new type of deformation mechanism map, such as evaluation and prediction of creep life, are discussed.

1. INTRODUCTION

The idea of representing the deformation behavior of materials in a 2-D map format was first put forward by Weertman and Weertman (1) in 1968. The basic principle of such type of representation is to keep all the deformation parameters except two constant and to assign the x and y axis to the remaining two variable parameters. The relationship between x and y and between x and y and the parameters that are kept constant is established by using the best available constitutive equations to describe each of the operative deformation mechanisms so that the x-y plane is divided into fields and within each field a single mechanism is rate-controlling.

To date, there are three basic types of 2-D deformation mechanism maps, namely,

- a. Stress-Temperature Maps. In this type of map the logarithm of the normalized stress, τ/G (τ = stress and G = shear modulus compensated for temperature), is plotted as a function of the homologous temperature, T/T_M (T = temperature in $^{\circ}\text{K}$ and T_M = absolute melting temperature), at constant grain size. This is the form originally proposed by Weertman (1) and later developed in detail by Ashby (2). Recently, Langdon and Mohamed (3) developed an alternative stress-temperature map by plotting the normalized stress against the reciprocal of homologous temperature. The advantage of such plots is that, for high temperature deformation mechanisms, all the field boundaries are straight lines, whereas in "Ashby-type" maps the field boundaries between mechanisms having different temperature dependence are curved and their construction requires extensive calculations.

- b. Grain Size - Stress Maps. This type of map, in which the normalized grain size, d/b (d = grain size and b = Burgess vector), is double logarithmically plotted against normalized stress, τ/G , at constant temperature, was introduced by Mohamed and Langdon (4).
- c. Grain Size - Temperature Map. Langdon and Mohamed (5) introduced this type of map where normalized grain size, d/b , is plotted against the reciprocal of homologous temperature, T_M/T , at constant stress.

In addition to the basic types of maps, specialized types of maps are possible such as ones incorporating microstructural details, i.e., obstacle spacing, effect of cold work, amount of precipitation, effect of impurities, effects of irradiation, etc.

A common characteristic for all types of maps is that they are constructed by using the best available constitutive equations. Consequently, they are limited by our understanding of flow processes in materials, i.e., the existing constitutive equations. Nonetheless, they are useful. Despite many approximations in their construction, they were successfully used to study the effect of crystal structure and atomic bonding on plastic flow characteristics of the materials, to search for missing mechanisms, to design experiments and interpret their results, to predict the mechanical behavior of materials for which only limited mechanical data is available, to study the effect of various strengthening mechanisms and, hence, to help in alloy design, in the selection of engineering materials for applications for which no previous experience is available, in the design of components where plastic flow during service is expected, flow of earth mantle, etc. (2, 6-12).

The purpose of this paper is two-fold: (i) to summarize experimental data on the high temperature deformation behavior of the Zn-22%Al alloy in the form of 2-D maps; and (ii) to present methods of construction and use of 3-D maps using the experimental data for this alloy as a prototype example.

2. EXPERIMENTAL DATA FOR Zn-22%Al ALLOY

Round, solid torsion specimens were machined from high (99.99%) purity Zn-22%Al eutectoid alloy plates with their longitudinal axis parallel to the direction of rolling. Before testing all the specimens were annealed at $528 \pm 2^\circ\text{K}$ for various lengths of time and resulted in grain sizes ranging between 0.8×10^{-4} cm and 3.5×10^{-4} cm. Torsion tests were carried out at constant strain rates between $5.4 \times 10^{-5} \text{ s}^{-1}$ and $1.7 \times 10^0 \text{ s}^{-1}$ and temperatures between 413°K and 533°K .

The relation between the applied shear strain rate ($\dot{\gamma}$) and the steady-state shear stress (τ) was analyzed according to the expression proposed by Mukherjee et al. (13) for high temperature diffusion-controlled deformation mechanisms,

$$\frac{\dot{\gamma} kT}{D G b} = A \left(\frac{b}{d}\right)^p \left(\frac{\tau}{G}\right)^n \quad [1]$$

where G is the shear modulus at the test temperature, D is the appropriate diffusivity (either for grain boundary or for lattice self-diffusion), b is the Burgers vector, d is the grain size, p is the grain size dependence of the strain rate, n is the stress sensitivity, and kT has the usual meaning of Boltzman's constant times absolute temperature.

According to Equation [1], a deformation mechanism is uniquely determined by the values taken by four parameters p , n , A , and Q , where Q is given by $D = D_0 \exp (-Q/RT)$ where D_0 = pre-exponential factor, Q = activation energy, and R = gas constant. Our experimental results with Zn-22%Al alloy indicate that, within the strain rates, temperatures, and grain sizes investigated, four deformation mechanisms are operative, namely, Coble creep (14), Nabarro-Herring creep (15,16), superplastic creep (17), and dislocation climb (17).

The experimental data are shown in Figure 1, and the constitutive equations developed from these data are listed in Table 1. The data in Figure 1 were double logarithmically plotted as $\dot{\gamma}kT/D_{gb}Gb (D_{gb}/D_L)^a$ vs. (τ/G) , where D_{gb} and D_L are grain boundary and lattice diffusivities, respectively, and a is equal to zero for mechanisms where grain boundary diffusivity controls the deformation and equal to unity for those mechanisms where the deformation is controlled by the lattice diffusivity. In this way all the diffusion-controlled deformation mechanisms can be shown in one plot (13). At low stresses two deformation mechanisms are operative: Coble creep and Nabarro-Herring creep. The transition from one mechanism to another occurs at $d \geq 2 \times 10^{-4}$ cm or for $d = 3.5 \times 10^{-4}$ cm at $T \approx 500^\circ\text{K}$ (18). At intermediate stresses the superplastic creep is rate-controlling, the datum points falling onto parallel lines depending upon the grain size. At high stresses (dislocation climb) all the datum points converge into a single line regardless of the grain size.

TABLE 1
Constitutive Equations for High Temperature
Creep Mechanisms for Zn-22%Al Alloy

Creep Mechanism	Constitutive Equation
Coble	$\frac{\dot{\gamma}}{D_{ogb}} \frac{kT}{Gb} = 106 \left(\frac{b}{d}\right)^{2.5} \left(\frac{\tau}{G}\right)^{1.25} \exp\left(\frac{-13,100}{RT}\right) \quad [2]$
Nabarro-Herring	$\frac{\dot{\gamma}}{D_{ol}} \frac{kT}{Gb} = 80 \left(\frac{b}{d}\right)^{1.6} \left(\frac{\tau}{G}\right)^1 \exp\left(\frac{-28,300}{RT}\right) \quad [3]$
Superplastic	$\frac{\dot{\gamma}}{D_{ogb}} \frac{kT}{Gb} = 80 \left(\frac{b}{d}\right)^{2.2} \left(\frac{\tau}{G}\right)^2 \exp\left(\frac{-13,100}{RT}\right) \quad [4]$
Dislocation Climb	$\frac{\dot{\gamma}}{D_{ol}} \frac{kT}{Gb} = 5.7 \times 10^6 \left(\frac{\tau}{G}\right)^5 \exp\left(\frac{-28,300}{RT}\right) \quad [5]$

3. 2-D MAPS

3.1 Construction of the maps

The maps were constructed using the constitutive equations listed in Table 1 and by using the criterion of equivalency of strain rates for two pertinent mechanisms at the transition (3,4). The boundary of the fields (stress/temperature or grain size/stress), where a simple mechanism is rate-controlling, are obtained by equating pairs of the constitutive equations [2] through [5] (2,4).

Since the homologous temperature of the two phases (Al-rich and Zn-rich) present in this alloy are very different, the homologous temperature for the alloy, T_H' , was calculated as (19):

$$T_H' = V_\alpha (T_H)_\alpha + V_\beta (T_H)_\beta \quad [6]$$

where V_α and V_β are the volume fractions of Al-rich and Zn-rich phases, respectively, and were taken as 0.42 and 0.58, respectively. $(T_H)_\alpha$ and $(T_H)_\beta$ are the homologous temperatures for Al-rich and Zn-rich phases, respectively.

3.2 Discussion of the results

Figure 2a,b shows stress-temperature maps drawn for $d = 1.7 \times 10^{-4}$ cm and 3.5×10^{-4} cm, respectively. It is evident from Figure 2 that as the grain size increases the superplastic creep field shrinks, most notably at the higher temperatures. Also, with the increase in grain size Nabarro-Herring creep field expands rapidly, especially at high temperatures, whereas the dislocation climb field moves at lower stress levels.

The grain size-stress maps are shown in Figure 3a,b. At 443°K (Figure 3a) the superplastic creep field seems to extend to very large grain sizes. The very likely possibility that superplastic creep is still the rate controlling mechanism at grain sizes as coarse as several hundreds of microns is very intriguing. Recently Wei and Nix (20) observed superplasticity in an Pb-In alloy at grain sizes up to 200 μm (2×10^{-2} cm). Unfortunately, due to the impossibility of obtaining coarse grain sizes in this alloy (18) we were unable to check this feature experimentally. Also, notice that Nabarro-Herring creep is not operative at this temperature for $(d/b) < 10^5$. Increasing the temperature (Figure 3b), the superplastic creep field shrinks to lower grain size values, dislocation climb field moves to lower stress levels at the

expense of the superplastic creep field and Nabarro-Herring creep is now operative at $(d/b) = 10^4$ for $(\tau/G) = 10^{-4}$ (well within experimental range).

4. A THREE-DIMENSIONAL DEFORMATION MECHANISM MAP

From the foregoing discussion it is clear that 2-D deformation maps offer a simple but powerful tool for visual presentation of mechanical data. The main drawback of these maps is their lack of generality. One must construct many maps, even for limited ranges of stress, temperature, and grain size, in order to obtain the overall picture. Moreover, many useful details might be lost when many different maps had to be analyzed together. On the other hand, the type of correlation which includes all the information about the operative mechanisms in one plot, i.e., Figure 1, cannot be visualized.

One way to combine these two approaches is to construct three-dimensional (3-D) deformation mechanism maps. Although not so simple as the two-dimensional maps, it includes all the pertinent information about the operative deformation mechanisms in a simple plot and the mechanical data presented can be still visualized.*

Such a 3-D deformation mechanism map was constructed for Zn-22%Al eutectoid alloy, Figure 4, using the constitutive equations listed in Table 1 and the equations developed in the Appendix for the construction of 3-D maps. It is easily seen from Figure 4 that the space occupied by Coble creep decreases as the stress, temperature, and grain size increase,

* After this work was completed it was brought to our attention that a 3-D deformation mechanism map for Al has just been completed by Oikawa (25).

respectively. The opposite is true for dislocation climb creep and Nabarro-Herring creep. The space occupied by these mechanisms increases as the stress, temperature, and grain size all increase.

The space occupied by superplastic creep always decreases as the temperature increases, but at any one temperature there is always a grain size where the range of stress over which superplastic creep is the rate-controlling mechanism is maximum. The value of the grain size corresponding to the maximum range of stress increases as the temperature decreases. The same is true about the stress. Similarly, at any one temperature there is always a stress where the superplastic creep is the rate-controlling mechanism over a maximum range of grain size. The stress value corresponding to the maximum range of grain size increases as the grain size itself increases and as the temperature decreases.

These observations are important in the view of the fact that a small grain size (usually less than 10 μm) is considered a prerequisite for superplasticity (21,22), although superplastic behavior was also observed in materials having grain sizes much larger (20, 23-24). Inspection of Figure 4 reveals that the superplastic creep domain is limited, at large grain sizes, by Nabarro-Herring creep and dislocation climb at high temperatures, and Coble creep and dislocation climb at low temperatures, respectively. Then, one way to obtain superplasticity at larger grain sizes is to decrease the temperature. However, this approach is limited since at temperatures below $0.4 - 0.5 T_M$ the diffusion-controlled creep mechanisms are replaced by low temperature thermally activated dislocation glide mechanisms (not shown in Figure 4). Another way to increase the stress-temperature-grain size space where superplastic creep

is rate-controlling is to bring changes in substructure. Changes in substructure will modify the value of the parameter A in Equation [1] and, consequently, will displace the boundaries between the various creep mechanisms (Equations [A16] and [A17] in the Appendix). The only condition is that the changes in substructure should be such that A_i and A_j (Equations [A16] and [A17] in the Appendix) will vary in opposite directions, i.e., one will increase whereas the other will decrease, or at least if they will vary in the same direction the change in the A_i , A_j -values should not be proportional. In the 3-D map any combination of stress, temperature, and grain size determines uniquely a resulting strain rate (Equation [A15] in the Appendix). Therefore, one can imagine a dynamic situation where stress, temperature, and grain size all change with time (for example, a turbine bucket in a gas turbine engine). If we know the variation of stress, temperature, and grain size with time (for the first two variables these are design data and for the latter can be experimentally determined) and if we neglect the effects of mechanical and thermal fatigue, then one can follow on the 3-D map the variation of strain rate with time. This is important if the creep life is to be evaluated. Very often, in high temperature applications, the creep life of a component is limited by the strain approaching a value that cannot be tolerated rather than by occurrence of fracture during creep. Since the strain accumulated at a particular strain rate is equal to the steady-state strain rate, $\dot{\epsilon}_{ss}$, times the deformation time at this strain rate,* i.e.,

* This is not entirely correct if the expected service life is short. In this case, the strain accumulated during primary creep will make an important contribution to the total strain. However, for long service times considered here, Equation [8] is a reasonable approximation.

$$\epsilon = \dot{\epsilon}_{ss} \times t \quad [7]$$

and, since the total strain, ϵ_t , is the sum of the strains accumulated at each strain rate, i.e.,

$$\epsilon_t = \dot{\epsilon}_{ss} \times t_1 + \dot{\epsilon}_{ss} \times t_2 + \dots \dot{\epsilon}_{ss_i} \times t_i = \sum_1^i \dot{\epsilon}_{ss_i} \times t_i \quad [8]$$

then, the total strain at any particular time can be evaluated. Conversely, the time when a predetermined strain value is reached can be calculated.

Equation [8] indicates that serious errors might occur when the probability that more than a single creep mechanism may be operative is ignored and the strain is calculated assuming an unique creep mechanism for all stresses, temperatures, and grain sizes encountered in a specific application.

It should be emphasized, however, that the success of using this type of 3-dimensional map will depend critically on the accuracy of the constitutive equations used in the construction of the map.

5. SUMMARY

- a. Two types of 2-D deformation mechanism maps were constructed for Zn-22%Al eutectoid alloy using experimentally determined deformation parameters.
- b. The relations among the operative creep mechanisms were analyzed as a function of stress, temperature, and grain size.
- c. A new type of deformation mechanism map, three-dimensional, was introduced and the basic equations for its construction were developed.
- d. The usefulness of 3-D deformation mechanism maps for visual presentation of mechanical data in real life, dynamic situations was discussed.

AKNOWLEDGEMENT

This research was supported by a Grant (AFOSR-79-0069) from the Air Force Office of Scientific Research.

APPENDIX

Construction of 3-D Deformation Mechanism Maps

We assume that all the rate-controlling creep mechanisms operate independently and their constitutive equations are of the form of Equation [1], which is rewritten here for convenience.

$$\frac{\dot{\gamma}kT}{DGb} = A \left(\frac{b}{d}\right)^p \left(\frac{\tau}{G}\right)^n \quad [A.1]$$

But it was shown that:

$$D = D_0 \exp\left(\frac{-Q}{RT}\right) \quad [A.2]$$

and,

$$G = G_0 - (\Delta G)T \quad [A.3]$$

From the definition we used for the homologous temperature for the alloy, i.e.,

$$T_H' = V_\alpha (T_H)_\alpha + V_\beta (T_H)_\beta \quad [A.4]$$

we can write,

$$T_H' = V_\alpha \frac{T}{(T_M)_\alpha} + V_\beta \frac{T}{(T_M)_\beta} = T \left[\frac{V_\alpha}{(T_M)_\alpha} + \frac{V_\beta}{(T_M)_\beta} \right] = \frac{T}{T_M'} \quad [A.5]$$

where $(T_M)_\alpha$ and $(T_M)_\beta$ are the melting temperatures for α - and β -phase, respectively, and T_M' is the equivalent melting temperature for the alloy given by:

$$T_M' = \frac{(T_M)_\alpha (T_M)_\beta}{V_\alpha (T_M)_\beta + V_\beta (T_M)_\alpha} \quad [A.6]$$

Now we can introduce a set of new variables as follows:

$$X = \frac{\tau}{G} \quad [A.7]$$

$$Y = \frac{d}{b} \quad [A.8]$$

$$Z = \frac{T_M'}{T} \quad [A.9]$$

Introducing Equations [A.2], [A.3], [A.5] through [A.9] in Equation [A.1] we obtain

$$\frac{\dot{\gamma} k T_M' \exp\left(\frac{QZ}{RT_M'}\right)}{D_0 b (G_0 Z - GT_M')} = A \frac{X^n}{Y^p} \quad [A.10]$$

If we assume $D_0 b = D_0 b = D_0$, then we can write

$$\frac{k T_M'}{D_0 b} = K' \quad [A.11]$$

and

$$\Delta G T_M' = K'' \quad [A.12]$$

where K' and K'' will be material constants. Also, we can write

$$\frac{Q}{RT_M'} = K''' \quad [A.13]$$

where for a given material K''' can take only two values, depending upon the activation energy for creep (either that for lattice diffusion or that for grain boundary diffusion).

Introducing Equation [A.11] through [A.13] in Equation [A.10] and rearranging it, we obtain the general expression for the 3-D map as,

$$\frac{\dot{\gamma} K' \exp(K''' Z)}{G_0 Z - K''} = A \frac{X^n}{Y^p} \quad [A.14]$$

Any combination among X , Y , and Z now locates a point in the stress-temperature-grain size space and completely and uniquely determines its

resultant strain rate. If it is so desired, planes of constant strain rate can be superimposed on Figure 4, each plane of constant strain rate being given by the relation,

$$\dot{\gamma} = \frac{A}{K'} (G_0 Z - K'') \frac{\dot{\gamma}^n}{\dot{\gamma}^p} \exp (-K''' Z) \quad [A.15]$$

The boundaries separating the volumes occupied by the various rate-controlling mechanisms can be calculated as follows:

- a. The boundaries between the mechanisms having different dependence on temperature are given by the relation

$$\frac{A_i}{A_j} \frac{\dot{\gamma}_i^{n_i-n_j}}{\dot{\gamma}_j^{p_i-p_j}} \exp [(K_j''' - K_i''') Z] = 1 \quad [A.16]$$

The subscripts i and j represent distinct deformation mechanisms.

- b. The boundaries between the mechanisms having the same dependence on temperature are given by the relation

$$\frac{A_i}{A_j} \frac{\dot{\gamma}_i^{n_i-n_j}}{\dot{\gamma}_j^{p_i-p_j}} = 1 \quad [A.17]$$

REFERENCES

- 1 J. Weertman and J.R. Weertman, in "Physical Metallurgy," p. 793, Ed. J.W. Cahn, North-Holland Publishing Co., Amsterdam (1965).
- 2 M.F. Ashby, Acta Metall., 20 (1972) 887.
- 3 T.G. Langdon and F.A. Mohamed, J. Mat. Sci., 13 (1978) 1282.
- 4 F.A. Mohamed and T.G. Langdon, Metall. Trans., 5 (1974) 2339.
- 5 T.G. Langdon and F.A. Mohamed, Mat. Sci. Eng., 32 (1978) 103.
- 6 H.J. Frost and M.F. Ashby, in "Rate Processes in Plastic Deformation of Materials," p. 70, Eds. J.C.M. Li and A.K. Mukherjee, ASM, Metals Park, Ohio (1975).
- 7 M.F. Ashby, in "The Microstructure and Design of Alloys," Vol. 2, p. 8, The Institute of Metals and The Iron and Steel Institute, London (1973).
- 8 J.T.A. Roberts and J.C. Voglewede, J. Amer. Ceram. Soc., 56 (1973) 472.
- 9 M.F. Ashby and H.J. Frost, in "Constitutive Equations in Plasticity," p. 117, Ed. A.S. Argon, M.I.T. Press, Cambridge, Mass. (1975).
- 10 J. Gittus, "Creep, Viscoelasticity and Creep Fracture in Solids," John Wiley and Sons, New York (1975).
- 11 M.F. Ashby and R.A. Verrall, in "Creep of Engineering Materials and of the Earth," p. 59, Eds. A. Kelly et al., The Royal Society, London (1978).

- 12 T.G. Langdon and D.A. Miller, in "Applications of Materials for Pressure Vessels and Piping," p. 99, Ed. G.V. Smith, ASME, New York (1979).
- 13 A.K. Mukherjee, J.E. Bird, and J.E. Dorn, Trans. ASM, 62 (1969) 155.
- 14 R.L. Coble, J. Appl. Phys., 34 (1963) 1679.
- 15 F.R.N. Nabarro, in "Report of a Conference on Strength of Solids," p. 75, The Physical Society, London (1948).
- 16 C. Herring, J. Appl. Phys., 21 (1950) 437.
- 17 J.E. Bird, A.K. Mukherjee, and J.E. Dorn, in "Relation Between Microstructure and Properties," p. 255, Eds. D.G. Brandon and A. Rosen, Israel Universities Press, Jerusalem (1969).
- 18 A. Arieli, Ph.D. Dissertation, University of California, Davis (1979).
- 19 T.H. Alden, in "Treatise on Materials Science and Technology," Vol. 6, p. 226, Ed. R.J. Arsenault, Academic Press, New York (1975).
- 20 J.E. Wei and W.D. Nix, Scripta Metall., 13 (1979) 1017.
- 21 J.W. Edington, K.N. Melton, and C.P. Cutler, Prog. Mat. Sci., 21 (1976) 61.
- 22 A.K. Mukherjee, Ann. Rev. Mat. Sci., 9 (1979) 191.
- 23 P. Griffiths and C. Hammond, Acta Metall., 20 (1972) 935.
- 24 R.C. Gifkins, Metall. Trans., 7A (1976) 1225.
- 25 H. Oikawa, Scripta Metall., 13 (1979) 701.

LIST OF FIGURE CAPTIONS

- Figure 1 Double logarithmic plot of temperature normalized strain rate versus normalized stress.
- Figure 2 Stress-temperature 2-D deformation maps.
(a) $d = 1.7 \times 10^{-4}$ cm; (b) $d = 3.5 \times 10^{-4}$ cm;
experimental datum points shown by circles.
- Figure 3 Grain size - temperature 2-D deformation maps. (a) $T = 443^\circ\text{K}$;
(b) $T = 503^\circ\text{K}$; experimental datum points shown by circles.
- Figure 4 3-D deformation mechanism map constructed for Zn-22%Al alloy.

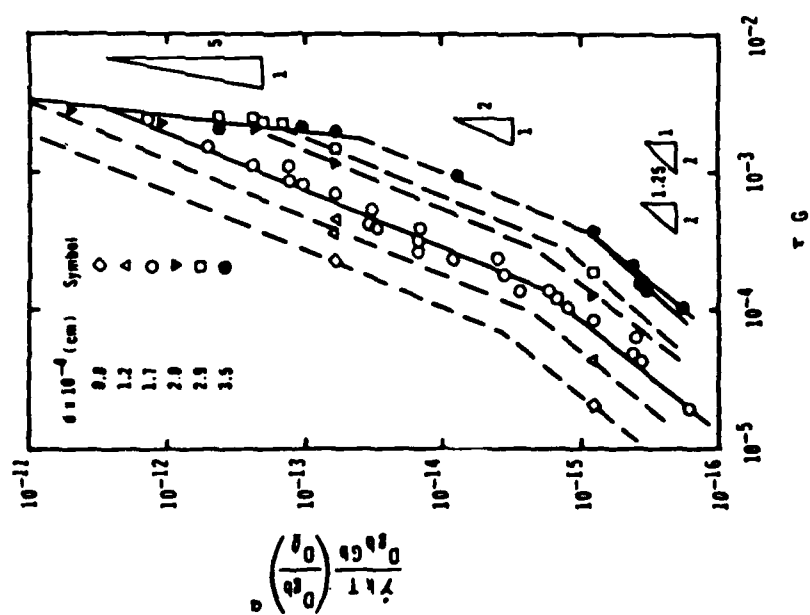


FIG. 1

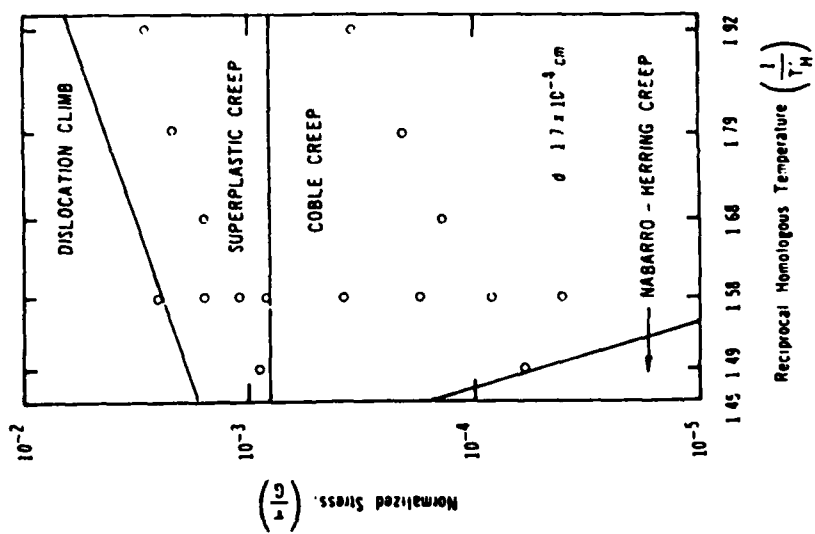


FIG. 2(a)

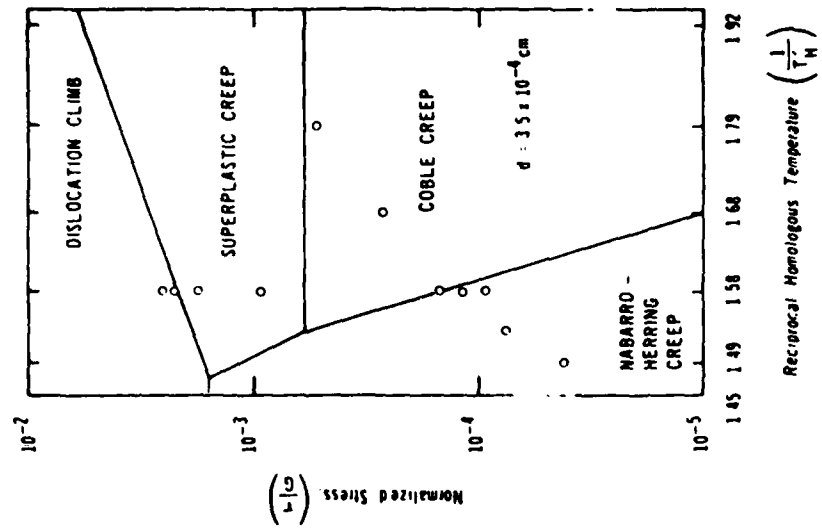


Fig 25)

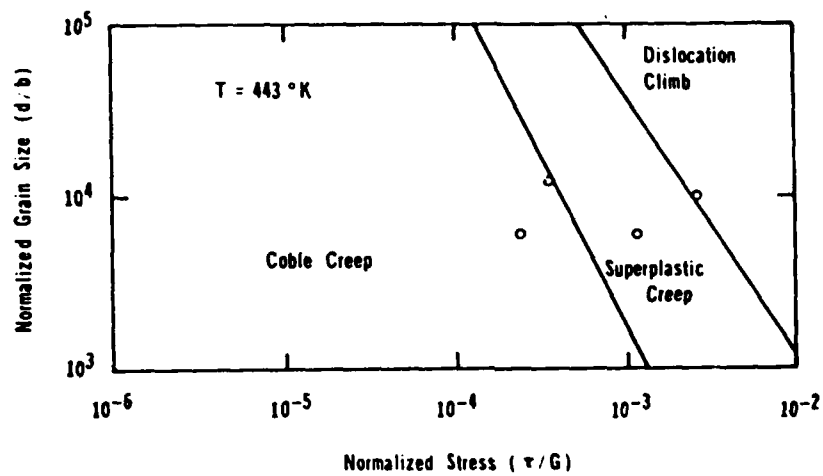


FIG 3(a)

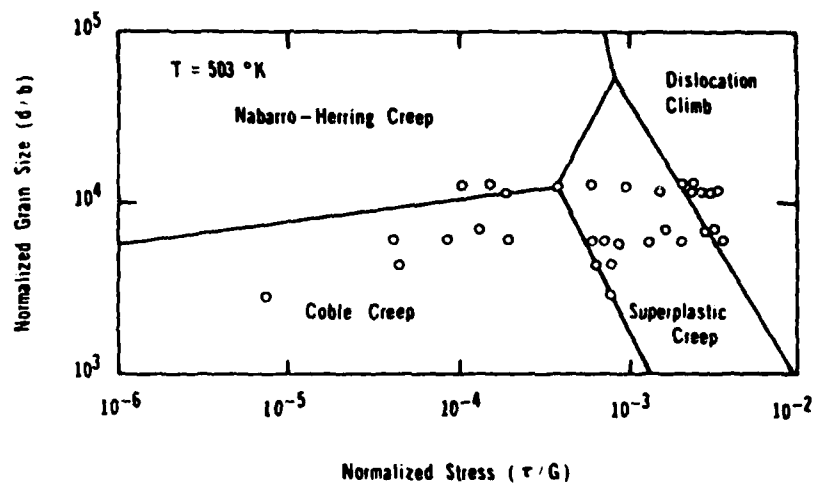


FIG. 3(6)

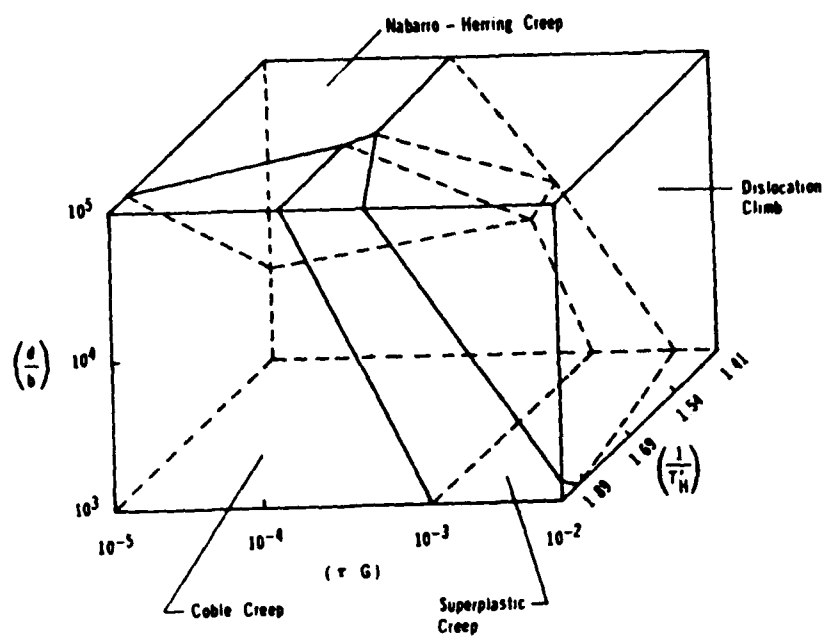


Fig. 4

SECTION 4.

LIST OF PUBLICATIONS RESULTING FROM AFOSR SUPPORT

1. A. Arieli and A. K. Mukherjee, "Factors Affecting the Ductility of the Superplastic Ti-6Al-4V Alloy," in "Strength of Metals and Alloys," p. 375, eds. P. Hassen et al, Pergamon Press, London (1979).
2. A. Arieli, A. K. S. Yu, and A. K. Mukherjee, "Low Stress and Superplastic Creep Behavior of Zn-22% Al Eutectoid Alloy," Met. Trans. A, 11A, 181 (1980).
3. A. Arieli and A. K. Mukherjee, "Factors Affecting the Maximum Attainable Ductility in Superplasticity," Mat. Sci. Engr., 43, pp. 47-54 (1980).
4. A. Arieli, B. J. Maclean and A. K. Mukherjee, "An Evaluation of the Effects of Concurrent Grain Growth During Superplastic Flow of the Ti-6Al-4V Alloy," published in the Proceedings of the Fourth International Conference on Titanium, Kyoto, Japan p. 1047, 1981.
5. A. Arieli and A. K. Mukherjee, High Temperature Creep Behavior of the Zn-22% Al Eutectoid Alloy," Acta Met., Vol. 28, p. 1571 (1980).
- 6-8 A. Arieli and A. K. Mukherjee, "High Temperature Creep of Zn-22 Al Eutectoid Alloy,"
 Part I - Mechanical Behavior
 Part II - Correlation
 Part III - Deformation Mechanism Maps
 presented at 109 AIME Annual Meeting, Las Vegas, Nevada (February 1980).
9. A. Arieli, "Investigation on Fundamental Aspects of Superplasticity," Ph.D. Dissertation, University of California, Davis (September 1979).
10. B. J. Maclean, "The Effect of Strain and Concurrent Grain Growth on the Superplastic Behavior of Ti-6Al-4V Alloy," M.Sc. Thesis, University of California, Davis (1980).
11. A. Arieli and A. K. Mukherjee, "Two and Three Dimensional Maps for the High Temperature Creep of Zn-22 Al Alloy," Materials Science and Engineering, vol. 47, p. 113-120, 1981.

SECTION 5

LIST OF PERSONNEL INVOLVED IN THE RESEARCH

1. A. K. Mukherjee - Professor of Materials Science, Department of Mechanical Engineering and Director, Materials and Devices Research Group, University of California, Davis, CA 95616.
2. A. Arieli - Post-Doctoral Research Associate, Department of Mechanical Engineering, University of California, Davis, CA 95616. Now at Olin Corporation, New Haven, CT.
3. B. J. Maclean - Research Assistant, Department of Mechanical Engineering, University of California, Davis, CA 95616. Now at Martin-Marietta Corp., Denver, Colorado.
4. G. Gurewitz - Post-graduate Research Engineer and Ph.D. Candidate, Division of Materials Science and Engineering, Dept. of Mechanical Engineering, University of California, Davis, CA 95616.

SECTION 6

LIST OF COUPLING ACTIVITIES WITH OTHER GROUPS

- a) Dr. Howard Hamilton
Dr. Amit Ghosh
North American Science Center
Thousand Oaks, CA
- b) Dr. H. Sastri
Dr. A. Yolton
McDonald Douglas Corp.
St. Louis, MO.
- c) ManTech Fabrication Group
Airplane Division
Northrop Corporation
Hawthorne, CA

FILME
— 8